

Stapp Car Crash Journal, Vol. 52 (November 2008), pp.
Copyright © 2008 The Stapp Association

Investigation of Traumatic Brain Injuries Using the Next Generation of Simulated Injury Monitor (SIMon) Finite Element Head Model

Erik G. Takhounts, Stephen A. Ridella
National Highway Traffic Safety Administration (NHTSA)

Vikas Hasija
GESAC Inc.

Rabih E. Tannous, J. Quinn Campbell, Dan Malone
AASA Inc.

Kerry Danelson, Joel Stitzel
Wake Forest University

Steve Rowson, Stefan Duma
Virginia Tech

ABSTRACT – The objective of this study was to investigate potential for traumatic brain injuries (TBI) using a newly developed, geometrically detailed, finite element head model (FEHM) within the concept of a simulated injury monitor (SIMon). The new FEHM is comprised of several parts: cerebrum, cerebellum, falx, tentorium, combined pia-arachnoid complex (PAC) with cerebro-spinal fluid (CSF), ventricles, brainstem, and parasagittal blood vessels. The model's topology was derived from human computer tomography (CT) scans and then uniformly scaled such that the mass of the brain represents the mass of a 50th percentile male's brain (1.5 kg) with the total head mass of 4.5 kg. The topology of the model was then compared to the preliminary data on the average topology derived from Procrustes shape analysis of 59 individuals. Material properties of the various parts were assigned based on the latest experimental data. After rigorous validation of the model using neutral density targets (NDT) and pressure data, the stability of FEHM was tested by loading it simultaneously with translational (up to 400 g) combined with rotational (up to 24,000 rad/s²) acceleration pulses in both sagittal and coronal planes. Injury criteria were established in the manner shown in Takhounts et al. (2003a). After thorough validation and injury criteria establishment (cumulative strain damage measure – CSDM for diffuse axonal injuries (DAI), relative motion damage measure – RMDM for acute subdural hematoma (ASDH), and dilatational damage measure - DDM for contusions and focal lesions), the model was used in investigation of mild TBI cases in living humans based on a set of head impact data taken from American football players at the collegiate level. It was found that CSDM and especially RMDM correlated well with angular acceleration and angular velocity. DDM was close to zero for most impacts due to their mild severity implying that cavitation pressure anywhere in the brain was not reached. Maximum principal strain was found to correlate well with RMDM and angular head kinematic measures. Maximum principal stress didn't correlate with any kinematic measure or injury metric. The model was then used in the investigation of brain injury potential in NHTSA conducted side impact tests. It was also used in parametric investigations of various "what if" scenarios, such as side versus frontal impact, to establish a potential link between head kinematics and injury outcomes. The new SIMon FEHM offers an advantage over the previous version because it is geometrically more representative of the human head. This advantage, however, is made possible at the expense of additional computational time.

KEYWORDS – Brain, finite element analysis, FE model, SIMon, human head modeling

INTRODUCTION

Traumatic brain injuries (TBI) are still one of the major "diseases" in the United States and worldwide. The Centers for Disease Control (CDC, 2003)

estimate 50,000 to 75,000 deaths are caused by TBI in the United States annually with approximately another 1.5 million suffering from various head injuries. Motor vehicle crashes remain one of the

major causes of TBI in the US second only to falls (Rutland-Brown et al. 2006). Based on NASS-CDS analyses of frontal crashes (Eigen and Martin, 2005) fatalities attributable to head injuries are second only to fatalities attributable to thoracic region (Figure 1) with societal costs exceeding \$6 Billion.

Cost and Fatalities Attributable to Injury in Frontal Crashes
(NASS-CDS 1997-2003, MY 1998+ vehicles)

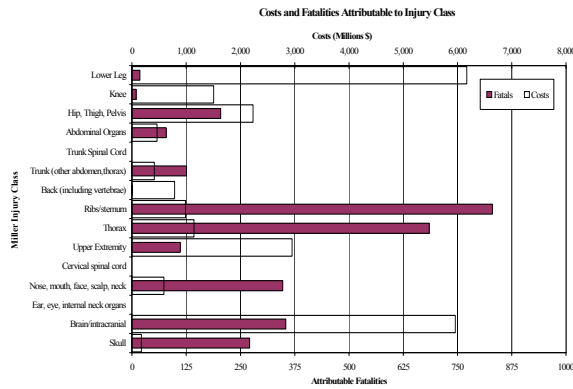


FIGURE 1. Cost and fatalities attributable to injuries in frontal crashes (Eigen and Martin 2005).

Many attempts have been made in the past to reduce the occurrence and severity of TBI as a result of automotive crashes. Among them are design and development of improved safety systems governed by various Federal Motor Vehicle Safety Standards (FMVSS). The process of further improvement of head injury protection systems is limited, however, by the degree of sophistication of currently used head injury assessment devices (test dummies) and associated injury criteria. Kinematic head injury criteria, based on various functions/functionals of measured head accelerations (e.g. head injury criterion - HIC), have served well in the past four decades to mitigate head injury. Relative mathematical simplicity of kinematic head injury criteria influenced their usefulness and worldwide acceptance. However, to take the next step forward in protecting automobile occupants from TBI, a better understanding of physical, biochemical, physiological and biomechanical processes within the traumatically injured brain is necessary. Finite element (FE) head models have been proven to be viable tools to better understand the biomechanics of TBI (Ruan et al. 1993, Bandak and Eppinger 1995, Bandak et al. 2001, Zhang et al. 2001, Kleiven et al. 2002, Takhounts et al. 2003a, Levchakov et al. 2006, Kleiven 2007). The NHTSA-developed Simulated Injury Monitor (SIMon) finite element head model (FEHM) is one of the available tools (Takhounts et al. 2003a) that uses crash dummy head kinematics as

an input to a FEHM, and calculates probability of three major types of brain injuries - diffuse axonal injury (DAI), focal lesions/contusions, and acute subdural hematoma (ASDH) - as an output. The 2003 version of SIMon used a relatively simple FEHM that allowed for a rather fast computation time at the expense of model's geometry. The model was thoroughly validated against various experimental data.

This paper introduces a new, more geometrically detailed, version of SIMon FEHM. It consists of major parts: cerebrum, cerebellum, falx, tentorium, combined cerebro-spinal fluid (CSF) and pia arachnoid complex (PAC), ventricles, brainstem, and parasagittal blood vessels. The model topology was derived from human computer tomography (CT) scans and then uniformly scaled such that the mass of the brain represents the mass of a 50th percentile male (1.5 kg) with the total head mass of 4.5 kg. The topology of the model was then compared to the preliminary data on the average cerebrum topology derived from Procrustes shape analysis (Bookstein 1996, Bookstein 1997, Gunz et al. 2005, Slice 2005, Slice and Stitzel 2004) of several human CT scans. Material properties of the various parts were assigned based on the latest experimental data (based on review by Kleiven 2007 and Takhounts et al. 2003b). The model was evaluated using available experimental data (Hardy et al. 2001, Nahum et al. 1977, Trosseille et al. 1992). Numerical stability of the model was assessed based on the methodology given in Zhang et al. (2001). The model was stable for loading rates of up to 400 g of translational accelerations combined with 24,000 rad/s² of rotational acceleration in both sagittal and coronal planes. Injury criteria were established in the manner shown in Takhounts et al. (2003a). After thorough validation and injury criteria establishment (cumulative strain damage measure - CSDM for DAI, relative motion damage measure - RMDM for ASDH, and DDM for contusions and focal lesions), the model was used in investigation of mild TBI cases in living humans based on a set of head impact data taken from American football players at the collegiate level. It then was used in the investigation of brain injury potential in NHTSA conducted side impact tests. It was also used in parametric investigations of various "what if" scenarios, such as side versus frontal impact, to establish a potential link between head kinematics and injury outcomes. The new SIMon FEHM offers a potential advantage over the previous version because it is geometrically more representative of the human head. This advantage, however, is made possible at the expense of additional computational time.

METHODS

Development of new SIMon FEHM

The topology of the SIMon FEHM is based on CT scans of a single male individual with the head size close to that of 50th percentile male. Detailed surfaces of the cerebrum, cerebellum, and brain stem were generated. Truegrid (XYZ Scientific Applications Inc., Livermore CA) software was used to develop a mesh of the skull, dura-CSF, and brain based on the outer brain surfaces. The SIMon FEHM consists of 42,500 nodes and 45,875 elements, of which 5153 are shell elements (3790 rigid), 14 are beam elements, and 40,708 are solid elements. This is a larger model compared to the previous (simpler) version of SIMon (10,475 nodes and 7,852 elements) and consequently requires more computing power

and time to run through the same loading event (10 hours on a high-end workstation for a 150 ms loading event versus 2 hours for the simpler SIMon).

Major parts of the brain were then created: cerebrum, cerebellum, brainstem, ventricles, combined CSF and pia arachnoid complex (PAC) layer, falx, tentorium, and parasagittal blood vessels (Figure 2). The PAC-CSF layer structurally represents the dura mater, arachnoid trabeculae, CSF, and pia mater. This layer is attached to the skull and the brain using common nodes. The foramen magnum was created with deformable shell elements to model the movement of the brainstem through the foramen magnum. The skull, falx cerebri, tentorium, and foramen magnum are represented with shell elements, and the bridging veins are made from beam elements, and the remaining parts used solid elements. Material models and properties used in the final version of the model are given in Table 1.

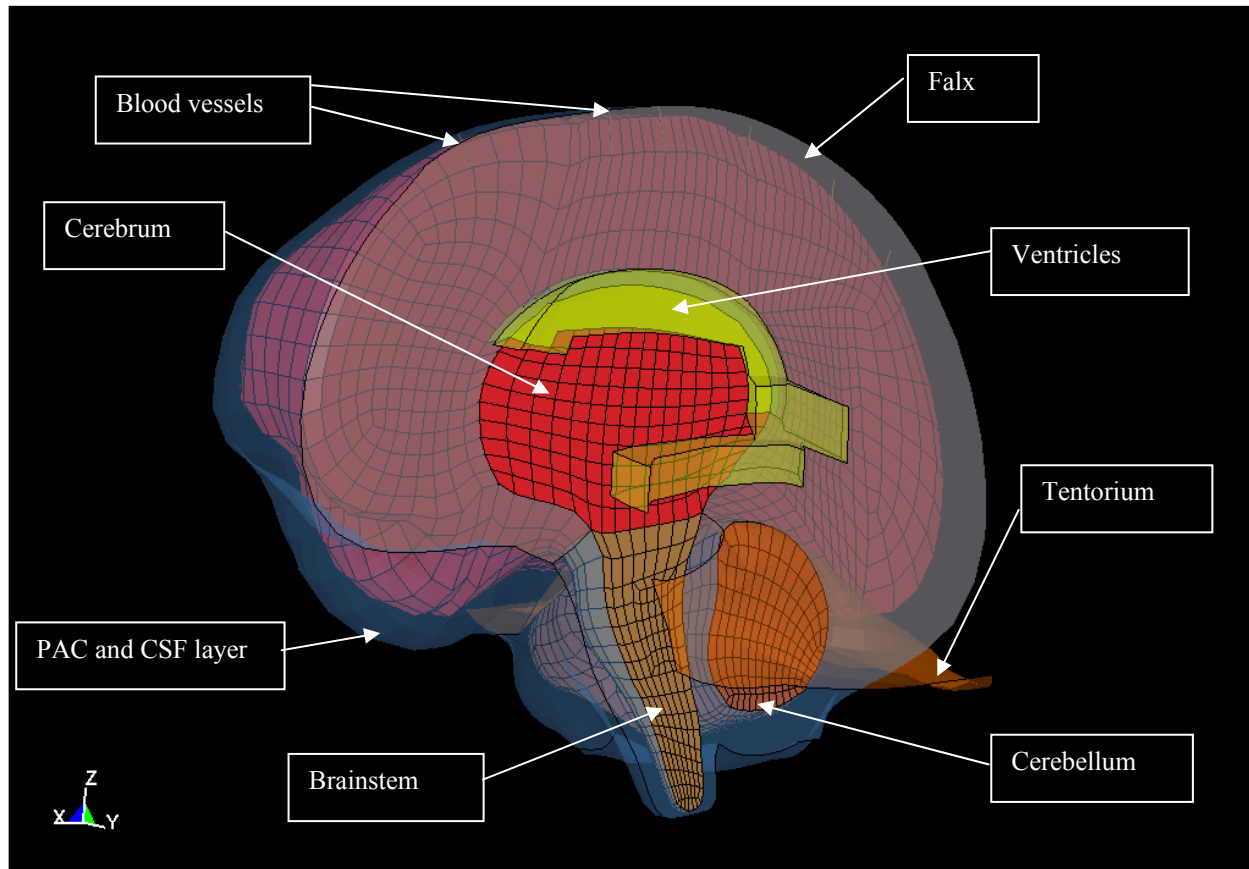


FIGURE 2. SIMon FEHM.

TABLE 1: Material models and properties used in SIMON FEHM.

Part	LS-Dyna Material Type	Material Properties
Cerebrum/ Cerebellum /Brain Stem	Kelvin- Maxwell Viscoelastic	$\rho = 1040 \text{ kg/m}^3$ $K = 558.47 \text{ MPa}$ $G_0 = 0.00166 \text{ MPa}$ $G_1 = 9.28\text{E-}04 \text{ MPa}$ $\beta = 16.95$
Ventricles	Elastic Fluid	$\rho = 1000 \text{ kg/m}^3$ $E = 0 \text{ MPa}$ $\nu = 0.5$ $K = 2100 \text{ MPa}$ $VC = 0.2$
Blood Vessels	Cable Discrete Beam	$\rho = 5000 \text{ kg/m}^3$ $E = 0.275 \text{ MPa}$
Falx- Tentorium	Elastic	$\rho = 1130 \text{ kg/m}^3$ $E = 31.5 \text{ MPa}$ $\nu = 0.45$
PAC-CSF	Kelvin- Maxwell Viscoelastic	$\rho = 1050 \text{ kg/m}^3$ $K = 4.966 \text{ MPa}$ $G_0 = 0.1 \text{ MPa}$ $G_1 = 0.02 \text{ MPa}$ $\tau = 0.01$
Foramen- Magnum	Elastic	$\rho = 1050 \text{ kg/m}^3$ $E = 6933.3 \text{ MPa}$ $\nu = 0.45$
Skull	Rigid	$\rho = 35,200 \text{ kg/m}^3$ $E = 6900 \text{ MPa}$ $\nu = 0.3$

ρ =Density, K =Bulk Modulus, G_0 = Short Time Shear Modulus, G_1 =Long Time Shear Modulus, β , τ = Decay Constant, E = Young's Modulus, ν = Poisson's Ratio, VC =Viscosity Coefficient.

The model was scaled uniformly (scaling ratio 0.96) such that the mass of the brain represented the mass of 50th percentile male (1.5 kg, brain density of 1040 kg/m³) with the total head mass of 4.5 kg. After scaling, the model's topology was compared to the preliminary data on average live adult human head topology derived from general Procrustes shape analysis (Bookstein 1996, Bookstein 1997, Gunz et al. 2005, Slice 2005, Slice and Stitzel 2004) of 59 individuals as described in Danelson et al. (2008). The individuals selected for this study ranged in age from newborn to 21 years of age with age groups at newborn, 3 months, 6 months, 1 year, 3 years, 6 years, 10 years, 15 years, and 21 years. The number of males and females in each group were evenly divided and the size of the individuals varied widely. One of the strengths of the general Procrustes analysis is the isolation of shape by removing variations in size prior to analysis.

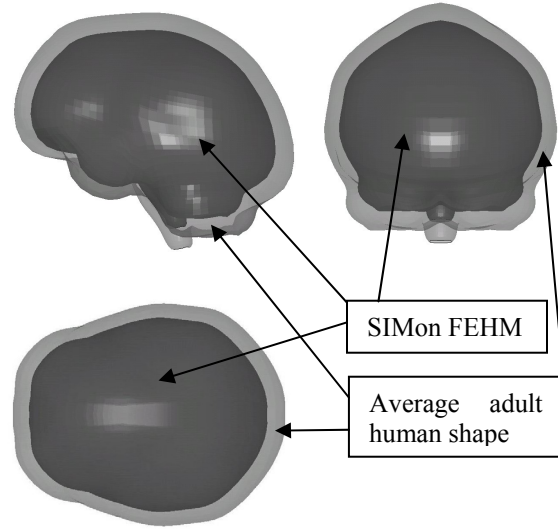


FIGURE 3. Shape of SIMon FEHM (darker gray) and shape of average adult human head (lighter gray) obtained from Procrustes shape analysis.

The model from this dataset was slightly larger (illustrated in light gray in Figure 3) than the scaled SIMon head (darker gray in Figure 3). To compare SIMon head shape to the shape derived from Procrustes dataset, an affine transformation was performed on the SIMon model along the x-, y-, and z-axis. The cerebrum scaling ratios calculated along these axes, as calculated in previous work, were used to scale the entire model (Danelson et al. 2008). The cerebrum scaling ratios were used since this structure changed the most with age and it is the largest structure in the model. The change in the size of these structures with age has been evaluated using the centroid size of the landmarks used for the Procrustes analysis and centroid size was expressed as a function of age.

Given a Procrustes analysis, standard statistical methods do not effectively assess significance since there are more variables than individuals. Therefore, to assess statistical significance of the cerebrum model a p-value was calculated using a permutation method (Good 2000, Gunz et al. 2005). The permutation test evaluates how many random combinations of coefficients found in the linear and quadratic regression models were a better predictor of landmark location than the model selected. Based on the permutation tests, the current Procrustes model showed high significance between landmark location given an age between newborn and 21 years old with a p-value of 0.00034 (Danelson et al. 2008). The shapes of the two models (SIMon and Procrustes method based human model) were very similar (Figure 3). However, the size of the individuals in the

dataset was not held constant; which may account for much of the difference between the models, since SIMON represents a 50th percentile individual.

There is no deficit of variability in the literature as far as brain material properties are concerned (Holbourn 1943, Koeneman 1966, Galford and McElhaney 1969, Fallenstein et al. 1969a, 1969b, Estes and McElhaney, 1970, Shuck and Advani 1972, Ljung 1975, Arbogast et al. 1995, Miller and Chinzei 1997, Donnelly and Medige 1997, Bilston et al. 1998, Darvish and Crandall 2001, Takhounts et al. 2003b, Nicolle et al. 2004). Constitutive models for brain tissue also vary in the literature – from simple linear elastic (Holbourn 1943, Koeneman 1966, Galford and McElhaney 1969, Fallenstein et al. 1969a, 1969b), through linear and quasi-linear viscoelastic (Estes and McElhaney, 1970, Shuck and Advani 1972, Ljung 1975, Arbogast et al. 1995, Miller and Chinzei 1997, Donnelly and Medige 1997, Bilston et al. 1998), Ogden rubber with linear viscoelastic component (Nicolle et al. 2004), to fully nonlinear Green-Rivlin models (Darvish and Crandall 2001, Takhounts et al. 2003b). This spectrum of choices for brain material models and properties makes the life of a head modeler hard and easy at the same time. Hard – because he/she still needs to select something out of a very large variety, and easy – because he/she can still find a reference for pretty much any model he/she chooses to use. Facing the uncertainty of brain material properties and models, a virtual shear test was conducted where different material models were used to compare their stress responses. A single element cube with dimensions 1x1x1 was created (Figure 4), simple shear displacement was applied (Figure 5) to one face of the element while the opposite face was fixed. Material properties used in this small study are given in Table 2. Shear stress response of the element was measured and compared (Figure 6). The criteria for choosing any particular set of properties were the SIMON FEHM’s response to the set of validation data (Hardy et al. 2001, Nahum et al. 1977, Trosseille et al. 1992) and the numerical stability runs.

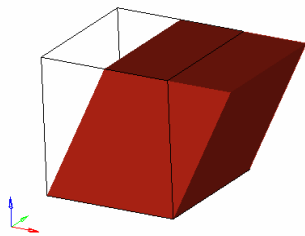


FIGURE 4. Single element cube used for the material study.

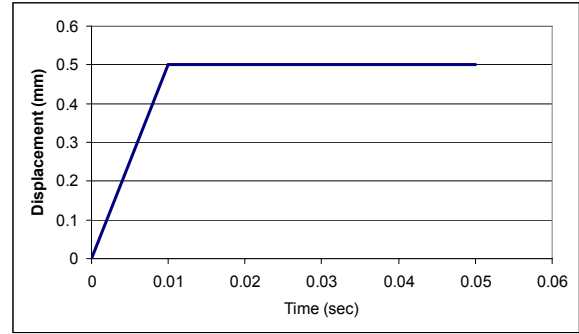


FIGURE 5. Displacement-time input applied to the single element model.

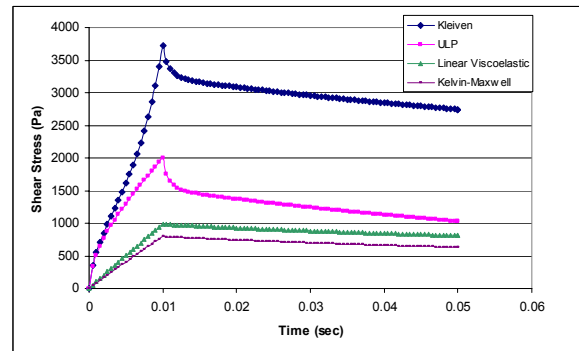


FIGURE 6. Shear stress output from a single element model for Klieven, ULP, Linear viscoelastic and Kelvin-Maxwell models.

Numerical stability of the model was tested based on the methodology described in Zhang et al. (2001), where a series of haversine translational (eq. 1a) and sinusoidal rotational accelerations (eq. 1b) were applied to the skull of the FEHM in both sagittal and coronal planes and the numerical model behavior was observed using the total, internal, and hourglass energies along with the observations of elements’ behavior.

$$a(t) = A_1 \left[1 - \cos\left(\frac{2\pi t}{T}\right) \right] \quad (1a)$$

$$\alpha(t) = \frac{2\pi A_2}{T} \sin\left(\frac{2\pi t}{T}\right) \quad (1b)$$

In equations 1a and b, A1 and A2 stand for the magnitude and T for period of the harmonic loading. Three magnitudes of loading conditions were used:

1. Peak linear acceleration = 200 g, and peak angular acceleration = 12,000 rad/s².

2. Peak linear acceleration = 300 g, and peak angular acceleration = 18,000 rad/s².

3. Peak linear acceleration = 400 g, and peak angular acceleration = 24,000 rad/s².

The validation of the FEHM consisted of two types of tests. The first type validated the strain field of the model based on the neutral density targets (NDTs) data presented by Hardy et al. (2001). In these tests the heads of post mortem human subjects (PMHS) were impacted in frontal, occipital, and temporal regions and the displacements of NDTs with respect to the skull were obtained using bi-planar x-ray system. The nodes closest to the location of each NDT were selected in the model and their displacements with respect to the skull calculated and compared to those obtained from PMHS. These calculations were performed for each of the material model given in Table 2. Three NDT tests: C383-T1 (frontal impact), C755-T2 (occipital impact), and C291-T1 (lateral impact) (Hardy et al. 2001) were selected for validation of the model because they ranged in the magnitude and direction of impacts. The second type of tests validated the stress field within the brain of SIMon FEHM and compared it to that obtained from PMHS tests of Nahum et al. (1977) and Trosseille et al. (1992). Once the stresses

and strains within the brain were validated against existing experimental data the injury criteria were established in the manner described in Takhounts et al. (2003a). It was assumed that the injury results from animal subjects were the same as that which would be observed from a human under the equivalent impact input. Three of the most common types of TBI (DAI, focal lesions/contusions, and ASDH) were simulated using their mechanical equivalents – CSDM for DAI, DDM for focal lesions/contusions, and RMDM for ASDH. Other mechanical measures, such as maximum principal stresses and strains, were also investigated. Data from animal experiments (Abel et al. 1978, Stalnaker et al. 1977, Nusholtz et al. 1984, Meaney et al. 1993) was used to determine critical values for each injury metric. In order to apply this data, the linear and angular kinematics recorded for the animals’ heads were scaled in magnitude and time to what a human head would experience (Takhounts et al. 2003a). These scaled kinematic time histories were then applied to the skull of SIMon FEHM, the injury metrics were computed from each test, and logistic regression was used to establish their critical values assumed to be at 50% probability. Receiver operating characteristic (ROC) curve for each injury measure was also calculated.

TABLE2: Material models and properties for brain tissue.

Ogden Rubber (Kleiven, 2007)		Ogden Rubber (ULP) (Nicolle et al., 2004)		Linear Viscoelastic (Takhounts et al., 2003b)		Quasi-Linear Viscoelastic (Takhounts et al., 2003b)		Kelvin-Maxwell Viscoelastic (Takhounts et al., 2003b)	
μ_1 (MPa)	5.38E-05	μ_1 (MPa)	0.06	G_1 (MPa)	9.276E-04	G_1 (MPa)	0.4	G_0 (Pa)	1662
μ_2 (MPa)	-1.204E-04	μ_2 (MPa)	0.00056	G_2 (MPa)	7.352E-04	G_2 (MPa)	0.41	G_1 (Pa)	928
μ_3 (MPa)	0.0	μ_3 (MPa)	0.00000125	G_3 (MPa)	3.876E-04	G_3 (MPa)	0.19	β	16.95
α_1	10.1	α_1	0.0451	β_1	0.0	β_1	0		
α_2	-12.9	α_2	-3.9	β_2	16.95	β_2	17.08		
α_3	0.0	α_3	16.3	β_3	1.17	β_3	1.05		
G_0 (MPa)	0.32	G_0 (MPa)	0.32			C_1 (MPa)	0.000985		
G_1 (MPa)	0.078	G_1 (MPa)	0.078			C_2 (MPa)	0		
G_2 (MPa)	0.0062	G_2 (MPa)	0.0062			C_3 (MPa)	0.03958		
G_3 (MPa)	0.008	G_3 (MPa)	0.008						
G_4 (MPa)	1E-04	G_4 (MPa)	1E-04						
G_5 (MPa)	0.003	G_5 (MPa)	0.003						
β_0	1000000	β_0	1000000						
β_1	100000	β_1	100000						
β_2	10000	β_2	10000						
β_3	1000	β_3	1000						
β_4	100	β_4	100						
β_5	10	β_5	10						

Investigating Potential for TBI in College Football Players

The helmets of ten college football players were instrumented with a newly developed 6 degree of freedom (6DOF) head acceleration measurement device (Simbex Inc., Lebanon, NH) for the 2007 American college football season. These sensors were capable of measuring linear and angular acceleration about each axis of the head for every head impact an instrumented player may experience during games and practices. The 6DOF sensor consisted of 12 single-axis, high-g accelerometers (ADXL193, Analog Devices, Norwood, MA) that were enclosed in padding and integrated into existing Riddell Revolution football helmets (Elyria, Oh). The sensor was designed so that the accelerometers remained in contact with the head at all times. This ensured that head acceleration, not helmet acceleration, was measured (Manoogian et al. 2006). In addition to the 12 accelerometers, the 6DOF sensor was equipped with on-board data acquisition and a wireless transceiver. Data acquisition was triggered anytime an accelerometer recorded 10 g's or more. Data was collected for 40 ms at 1000 Hz, of which 8 ms were pre-trigger and 32 ms were post-trigger. Each recorded impact was downloaded wirelessly by a sideline computer via the 6DOF sensor's transceiver. Linear and angular accelerations about the center of gravity of the head were computed from the raw skull acceleration measurements through post-processing using a novel algorithm (Chu et al. 2006). Since the system was over-defined with 12 accelerometers, the linear and angular acceleration at the head CG were optimized. The sensor and algorithm were validated to the head CG of the Hybrid III dummy through dynamic impact testing. A total of 1712 impacts were recorded. All data was up-sampled to 10 kHz by linear interpolation and then filtered to SAE J211 specification. Out of 1712 impacts the 24 most severe ones were selected for this study using the SIMon FEHM to assess the potential for TBI. None of the impacts resulted in brain or other head injury.

Frontal versus Side Impact

One of the interesting applications of any mathematical model is conducting parametric analyses and investigating hypothetical loading scenarios. Frontal versus side impact tolerance of the human head is one of these applications. Loading conditions similar to those described above for the numerical stability tests were applied to the model first in sagittal and then in coronal plane. The model response in each plane to the same loading conditions was compared using injury metrics: maximum

principal stress, maximum principal strain, CSDM, DDM, and RMDM.

NHTSA Conducted Side Impact Tests Evaluation

This section demonstrates potential use of the SIMon FEHM in evaluating vehicle performance using 3-dimensional head translational and rotational data measured in existing anthropometric test devices (ATDs) using a nine accelerometer array package. This translational and rotational data was applied to the skull of SIMon FEHM, brain injury metrics were computed and results were compared to the kinematic injury criteria – HIC. Two side impact tests were selected for demonstration purposes – one with side curtain airbag (case 1), the other without (case 2). Case 1 had HIC₁₅ value of 668, case 2 had it equal to 225. Translational/linear and angular accelerations time histories (all time histories in this paper are given in standard SAE sign convention) for each case are given in Figure 7.

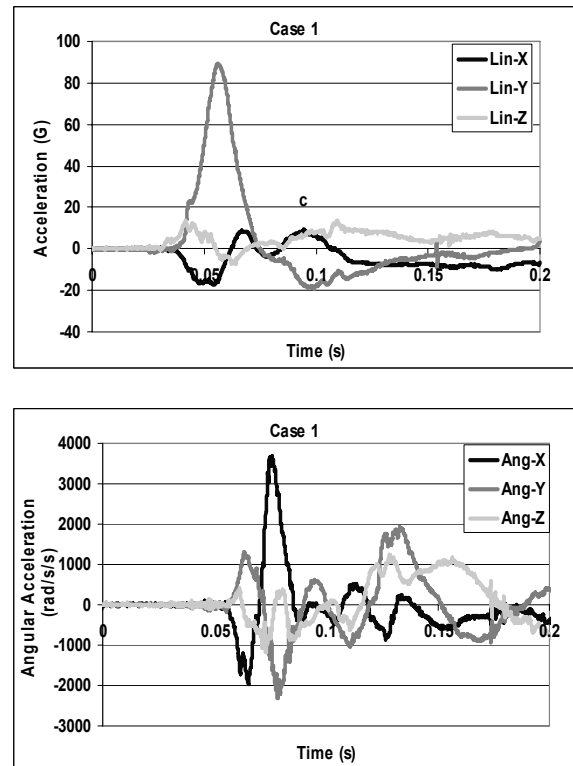


FIGURE 7. a) Linear and angular acceleration time histories for Case 1.

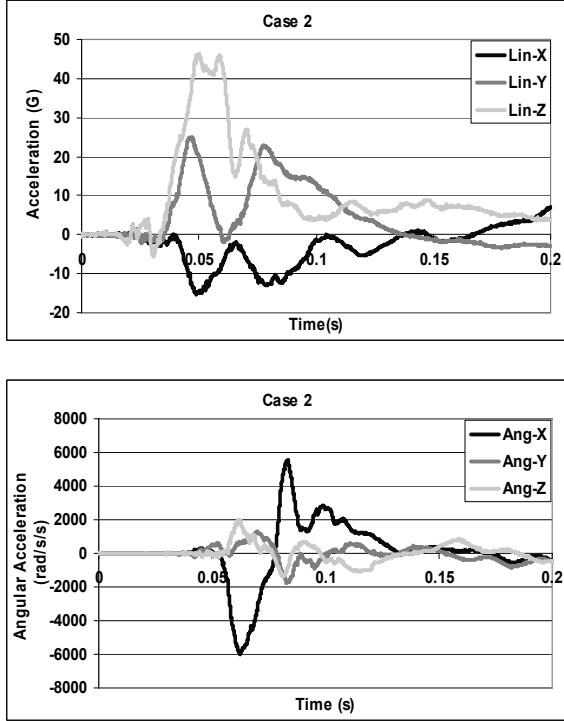


FIGURE 7. b) Linear and angular acceleration time histories for Case 2.

RESULTS

Development of SIMon FEHM

Shear stress responses computed from a single element study (Figure 6) showed that Kelvin-Maxwell model derived from Takhounts et al. (2003b) had the softest stress response among the four material models given in Table 1. Because of that response, it was expected to have more numerical stability issues with it when used in SIMon FEHM. The results, however, proved otherwise. For comparison, in Figure 8 (a) the results for the most severe loading condition 3 are shown for stiffest Ogden Rubber brain model used in Kleiven (2007) and in Figure 8 (b) the results for the same loading condition are shown for much softer Kelvin-Maxwell model derived from Takhounts et al. (2003 b). Although the model’s response with Kelvin-Maxwell brain material model showed greater ratio of the hourglass to internal (and total) energy compared to the model with Ogden Rubber brain material model (Table 3), the observation of unstable areas (Figure 8) anywhere in the model indicated superior stability of the model with Kelvin-Maxwell brain material model. The ratios of hourglass to total energies for both material models were very small and below the recommended level of 0.03 to 0.05 (Belytschko 1974, Belytschko and Kennedy 1978, Belytschko and Tsay

TABLE 3: Comparison of the hourglass to total energy ratios for two material types.

Loading Condition	<i>Hourglass Energy</i>	<i>Hourglass Energy</i>
	<i>Total Energy</i> (Ogden Rubber Material Model)	<i>Total Energy</i> (Kelvin-Maxwell Material Model)
Loading Condition 1	0.0022	0.0096
Loading Condition 2	0.0024	0.0091
Loading Condition 3	0.0026	0.01

1983, Belytschko and Bindeman, 1993, Belytschko et al., 2000), so Kelvin-Maxwell model was chosen because it was more stable and because it allowed direct computation of CSDM and DDM in LS-Dyna (Livermore CA).

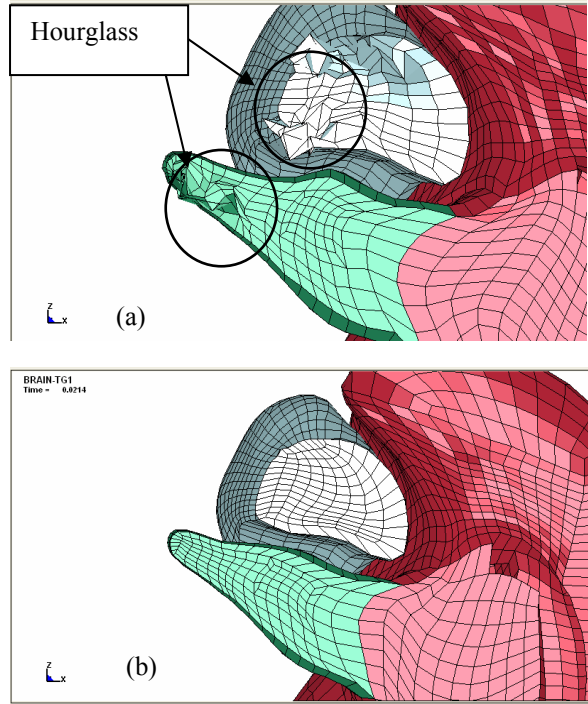
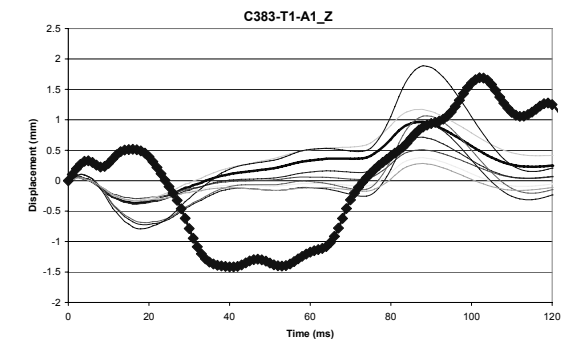
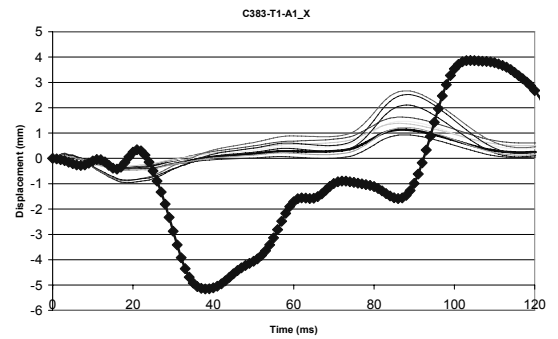
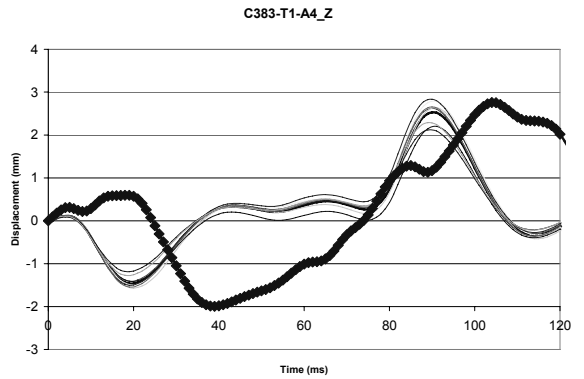
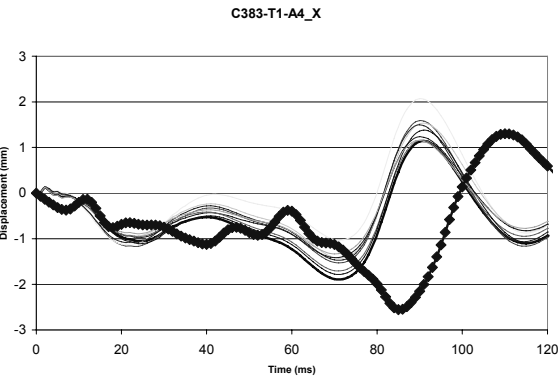
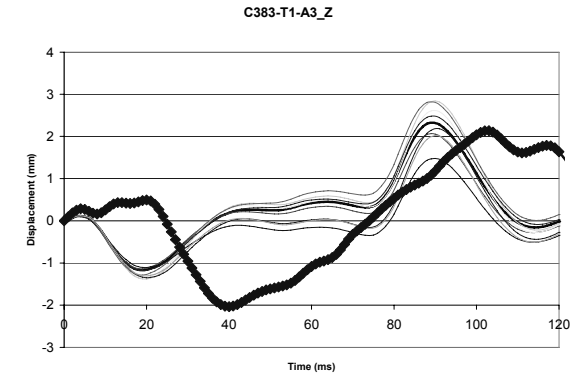
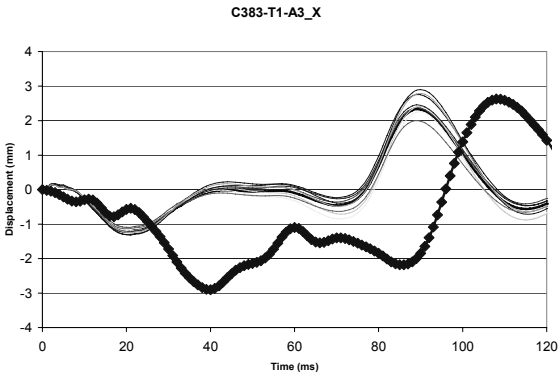
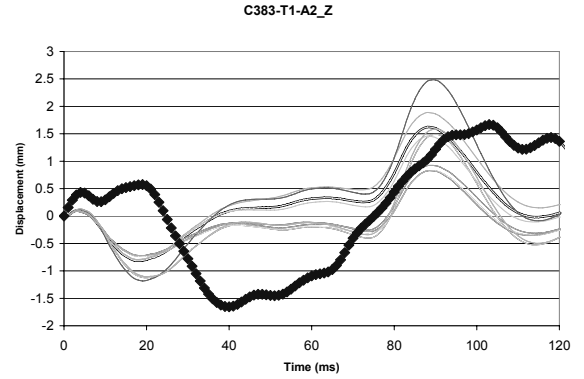
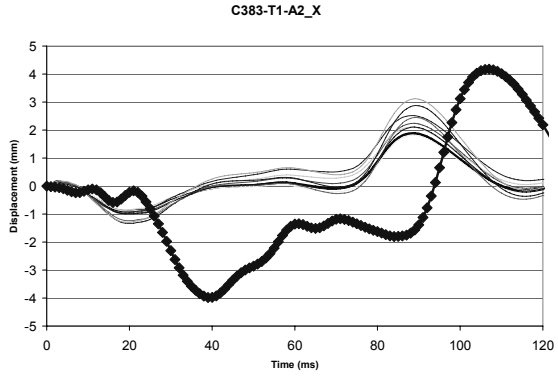


FIGURE 8. Stability runs for Ogden Rubber (a) and Kelvin-Maxwell (b) brain material models.

The displacement-time histories of each NDT for each test are shown in Figure 9 where the abscissa is the time in ms and the ordinate is the displacement in mm, the right column shows the displacement-time histories in Z-direction and left column shows the displacement-time histories in X-direction for frontal (Figure 9, a-c) and occipital (Figure 9, d-f) impacts and Y-direction for lateral (Figure 9, g-i) impacts.



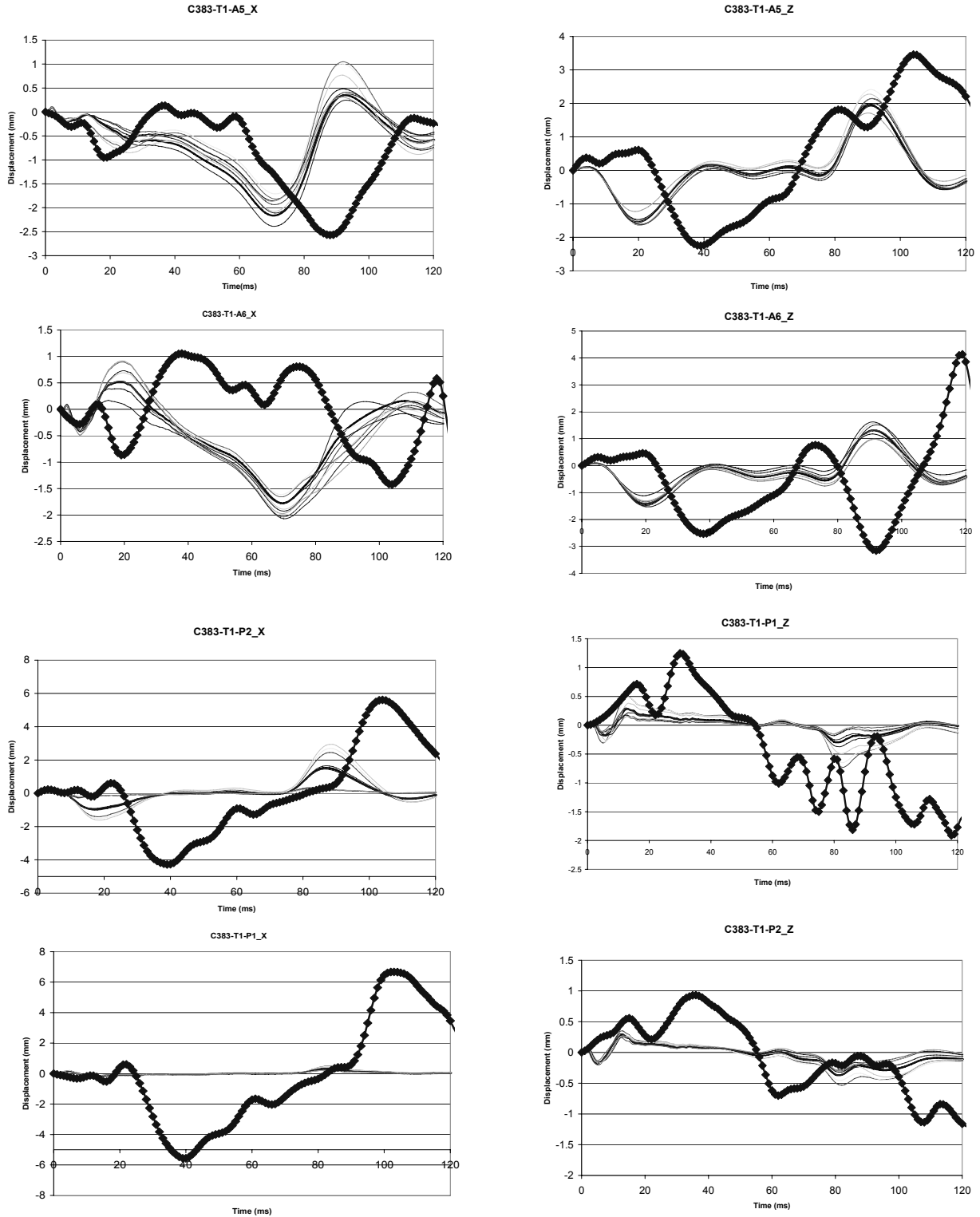
X-displacement

Z-displacement

█ Experimental

— Computational

a) C383-T1 (frontal impact): anterior NDTs A1 - A4 displacement-time histories.



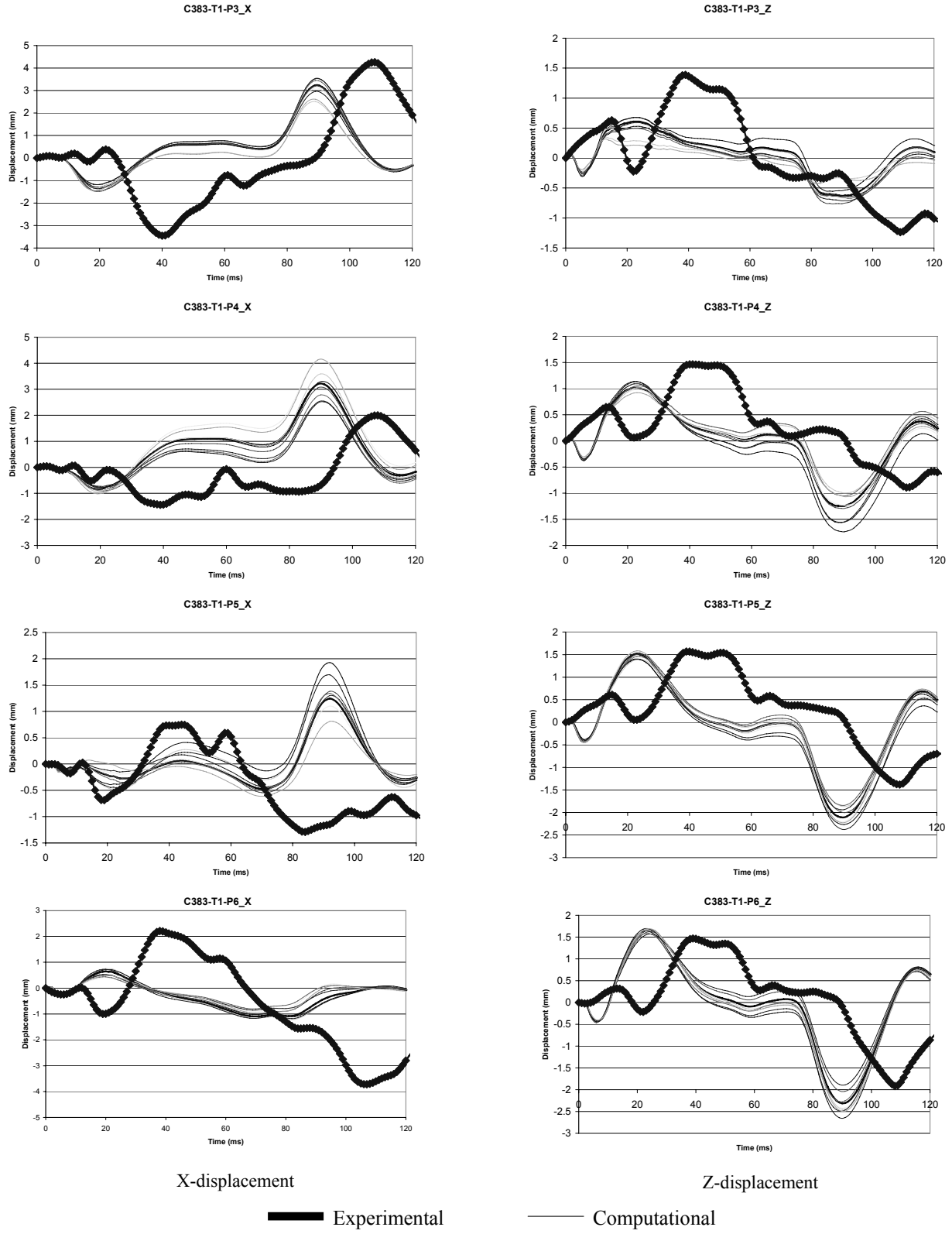
X-displacement

Z-displacement

— Experimental

— Computational

b) C383-T1 (frontal impact): anterior NDTs (A5, A6 – upper two rows) and posterior NDTs (P1, P2 – lower two rows) displacement-time histories.



c) C383-T1 (frontal impact): posterior NDTs (P3 – P6) displacement-time histories.

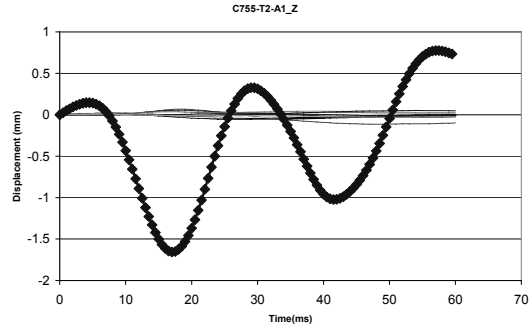
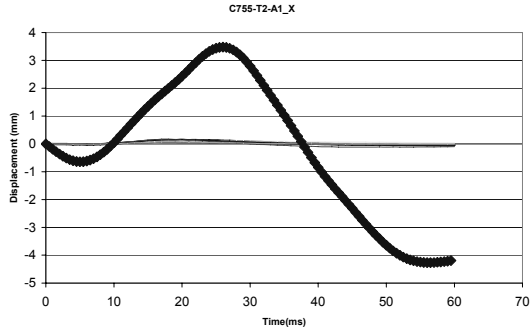
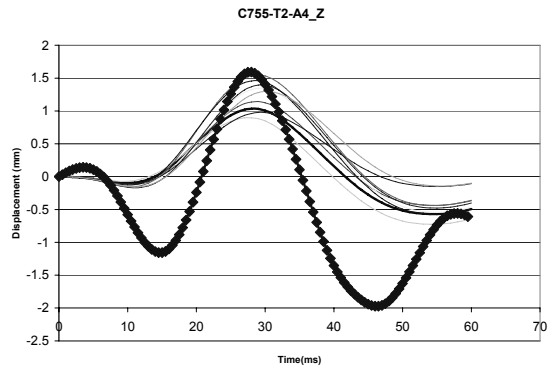
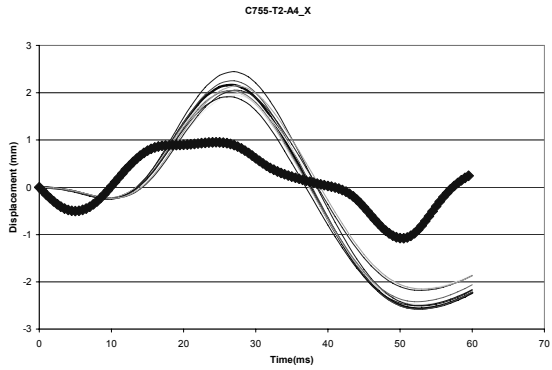
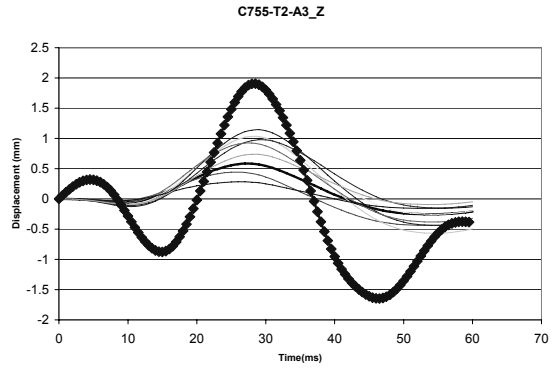
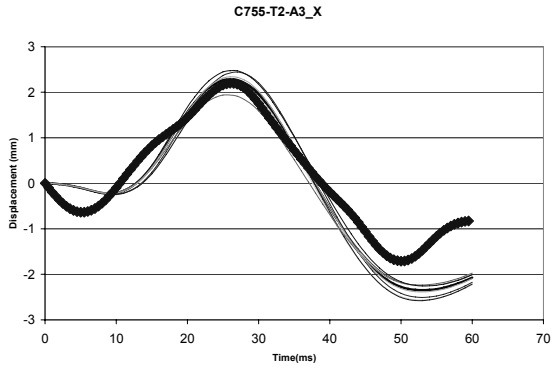
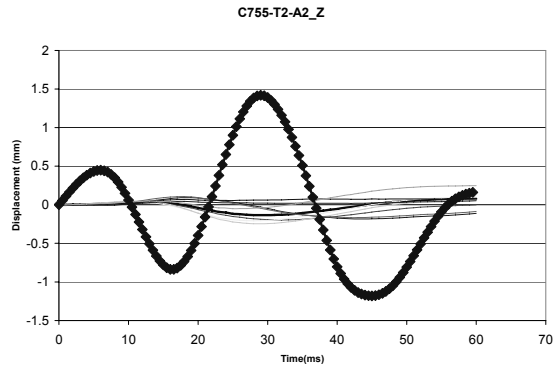
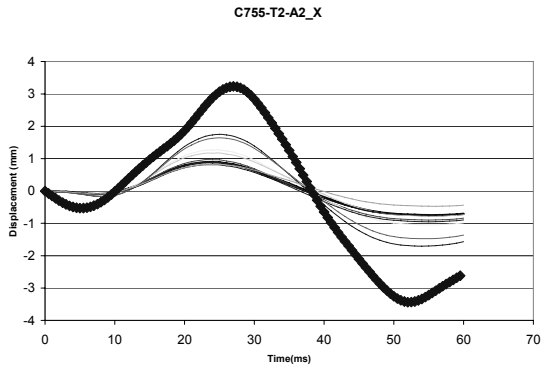


Figure B2. 383-T1-A1z



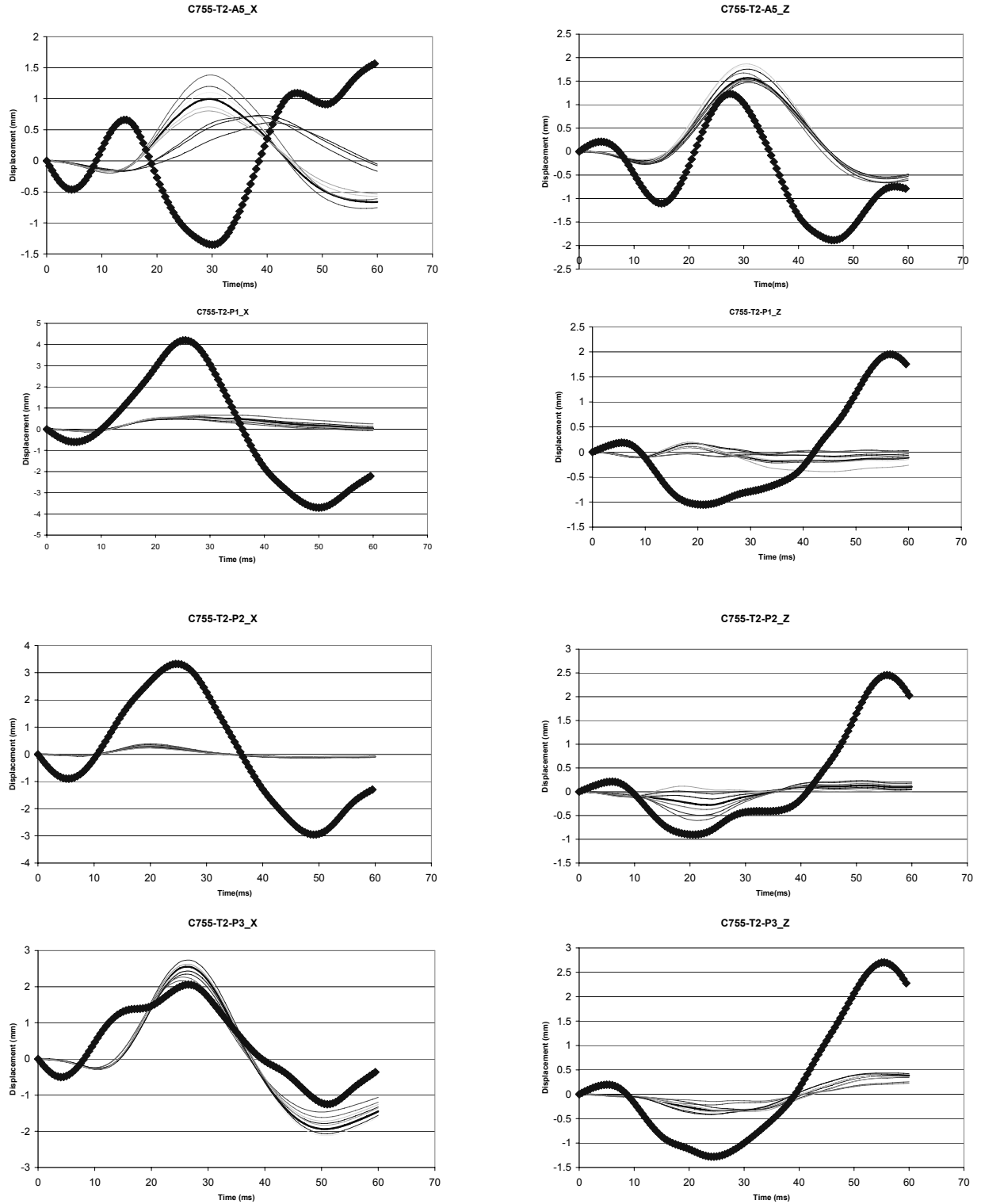
X-displacement

Z-displacement

— Experimental

— Computational

d) C755-T2 (occipital impact): anterior NDTs A1 - A4 displacement-time histories.



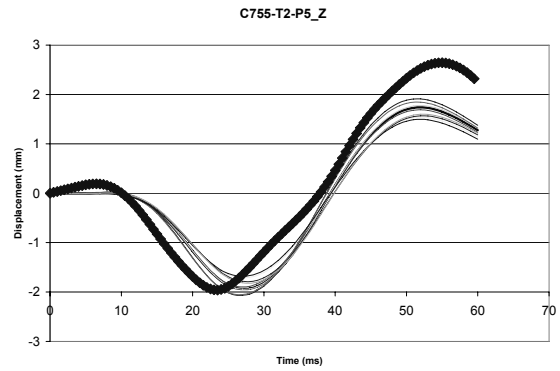
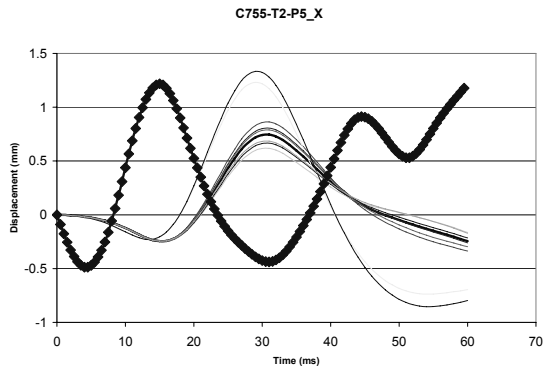
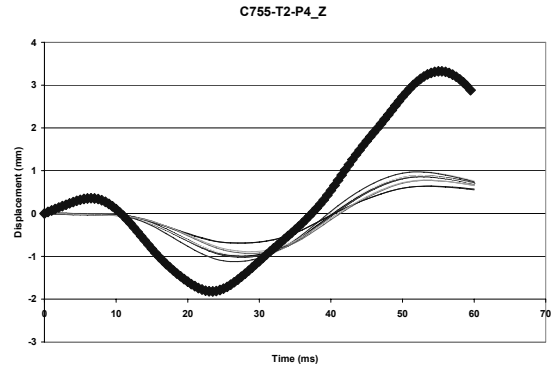
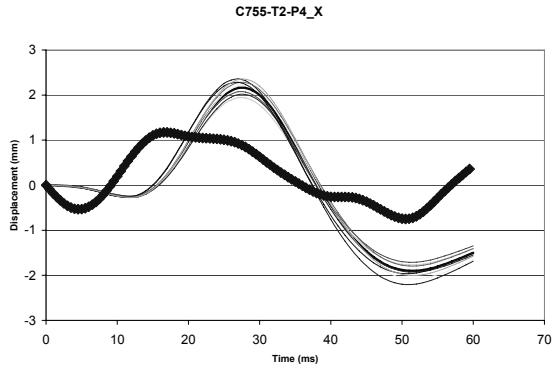
X-displacement

Z-displacement

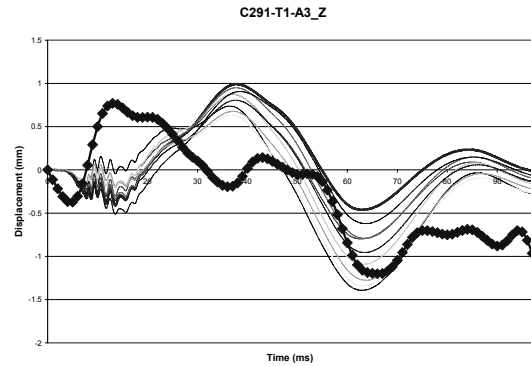
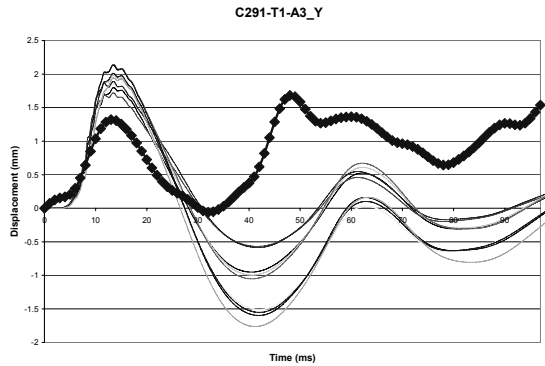
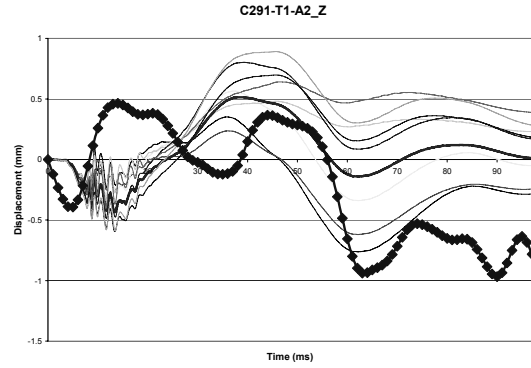
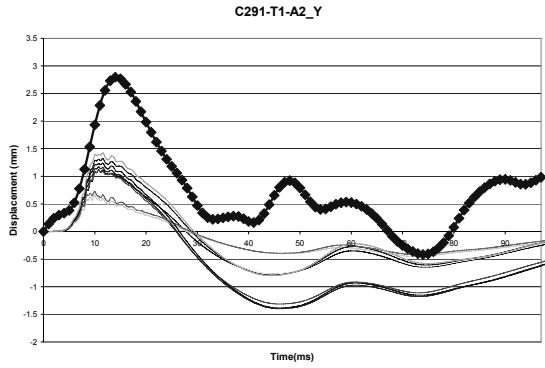
— Experimental

— Computational

e) C755-T2 (occipital impact): anterior NDT (A5 – upper row) and posterior NDTs (P1 – P3 – lower three rows) displacement-time histories.



f) C755-T2 (occipital impact): posterior NDTs P4 and P5 displacement-time histories.



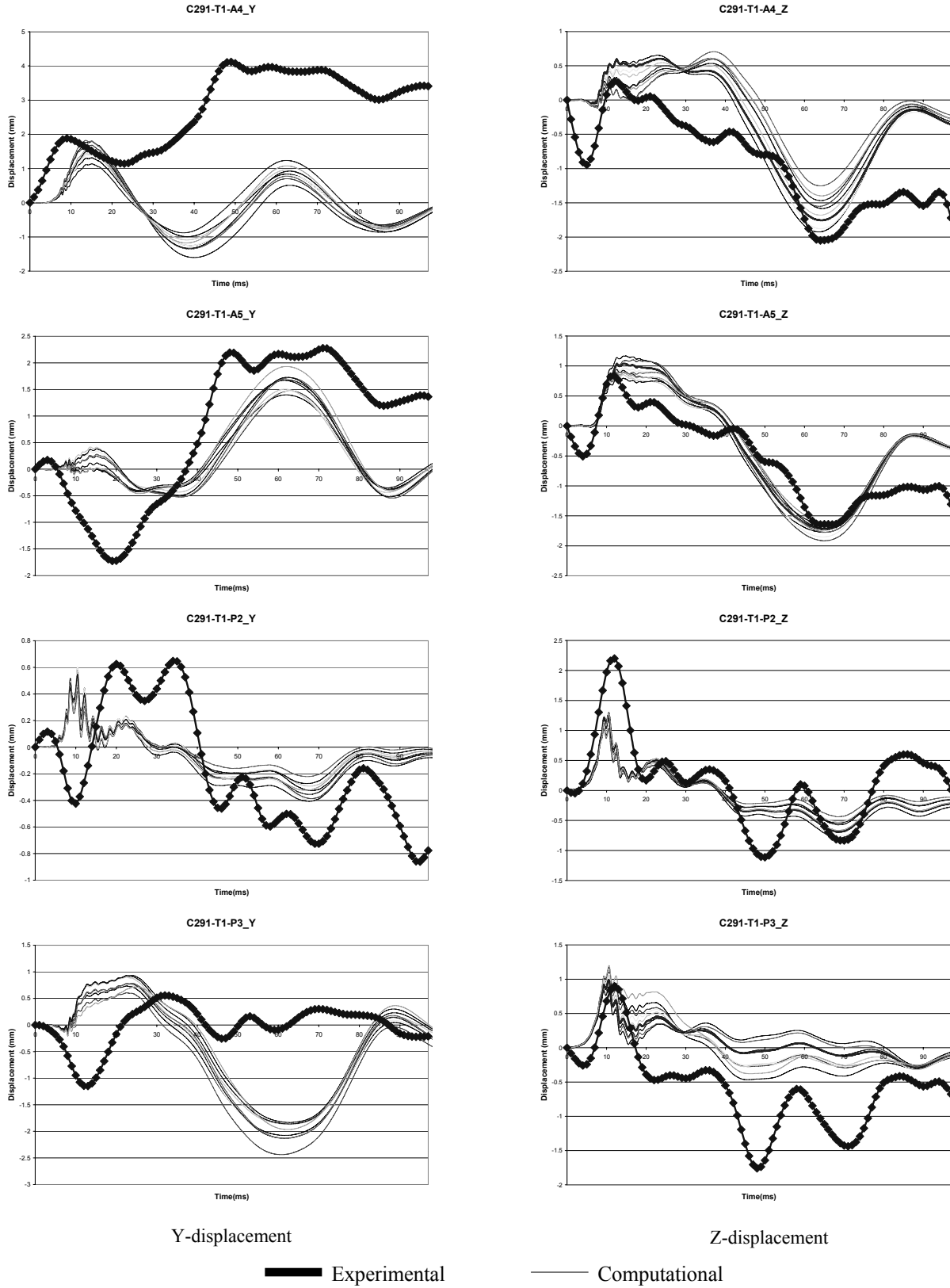
Y-displacement

Z-displacement

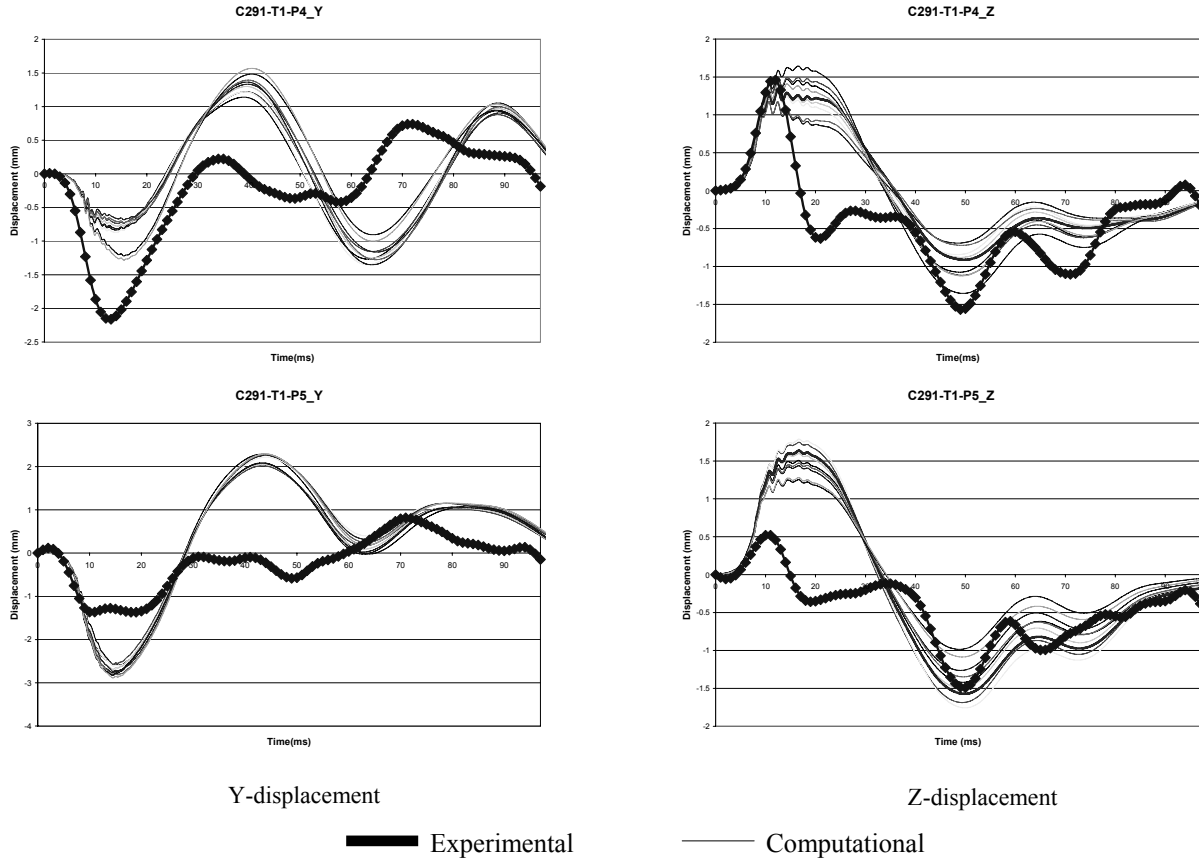
— Experimental

— Computational

g) C291-T1 (lateral impact): anterior NDTs A2 and A3 displacement-time histories.



h) C291-T1 (lateral impact): anterior NDTs (A4 and A5 – upper two rows) and posterior NDTs (P2 and P3 – lower two rows) displacement-time histories.



i) C291-T1 (lateral impact): posterior NDTs P4 and P5 displacement-time histories.

FIGURE 9. Hardy et al., 2001 NDT data: displacement-time histories – experiments and simulations.

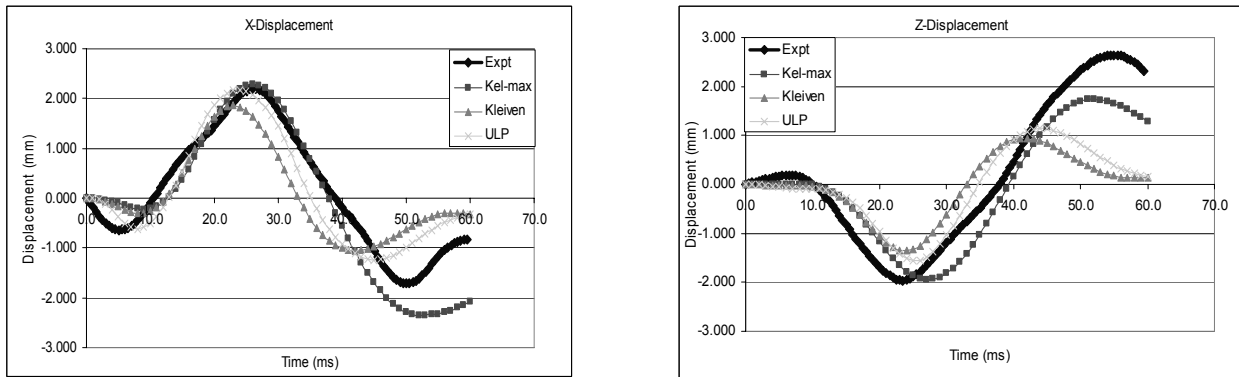


FIGURE 10. Hardy et al., 2001 NDT response for different brain material models and parameters.

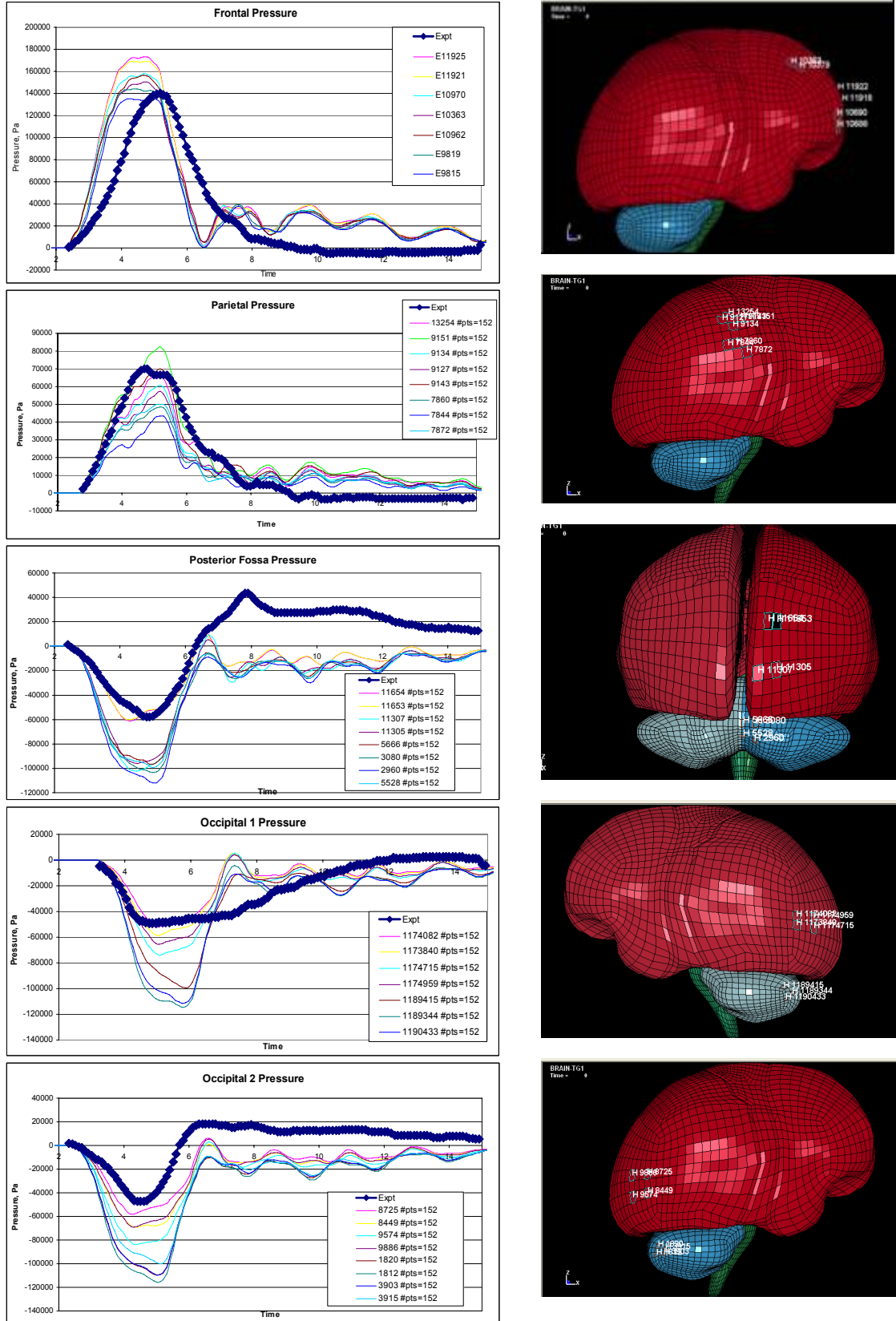


FIGURE 11. Nahum et al., 1977 test results: pressure-time histories at various brain locations and locations of pressure measuring elements in the model.

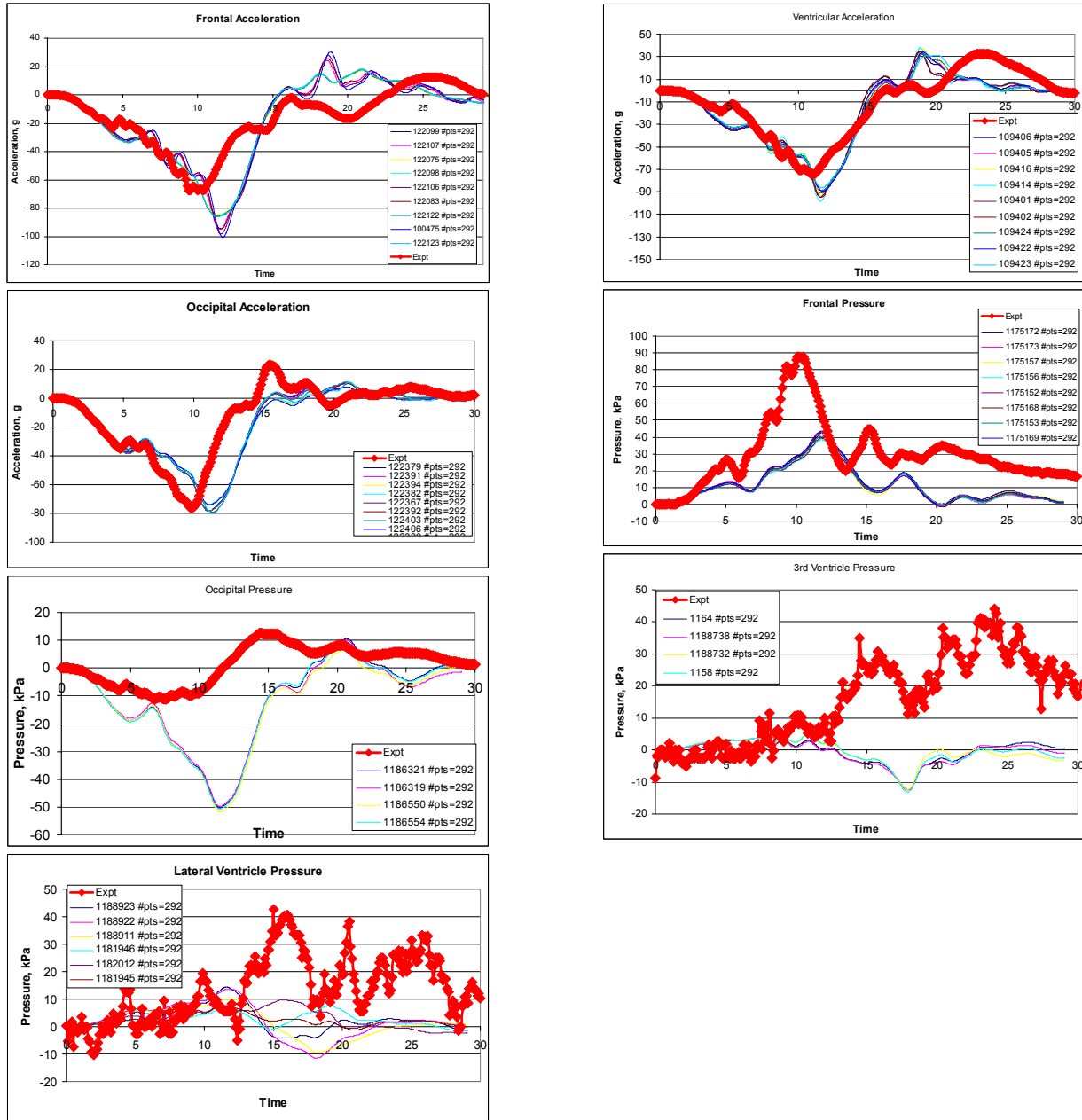


FIGURE 12. Trosseille et al. 1992 test results: pressure-time histories at various brain locations.

All displacements are expressed in the local skull coordinate system and measured with respect to the skull. Figure 10 gives an example of NDT responses for different brain material models and parameters given in Table 2. Pressure-time histories based on Nahum et al. (1977) tests are shown in the left column of Figure 11. Due to fairly high pressure gradients within the brain the measurements were taken from several locations in the model (right column) representing the approximate location of the pressure sensors reported in the paper by Nahum et al. (1977). Similarly, for Trosseille et al. (1992) test

data, pressure-time histories for various locations in the brain and ventricles were computed (Figure 12). Out of five investigated biomechanical measures (CSDM, DDM, RMDM, maximum principal stress and maximum principal strain) considered in this study only CSDM and maximum principal strain correlated with brain injuries (Figures 13 and 14) recorded in animal tests (Abel et al. 1978, Stalnaker et al. 1977, Nusholtz et al. 1984, Meaney et al. 1993). CSDM (0.25) indicates that the volume fraction of the brain is computed that exceeded the threshold of

maximum principal strain value of 0.25. 50% probability of DAI corresponded to 54% (Figure 13 a) of brain volume experienced at some point in the event maximum principal strain of 0.25 and above. Any probability (p) of DAI based on CSDM (0.25) can be computed using the following equation:

$$p = \frac{1}{(1 + e^{-7.860 * CSDM(0.25) + 4.236})}$$

The ROC curve, representing the fraction of true positives versus the fraction of false positives, for CSDM (0.25) is given in Figure 13 b.

Probability of DAI based on maximum principal strain can be computed from:

$$p = \frac{1}{(1 + e^{-3.759 * Max Pr in Strain + 3.286})}$$

50% probability of DAI corresponds to the maximum principal strain value of 0.87 (Figure 14 a) experienced anywhere in the brain at any point in the mechanical event. ROC curve for maximum principal strain is shown in Figure 14 b. Both injury measures were developed based on 68 observations.

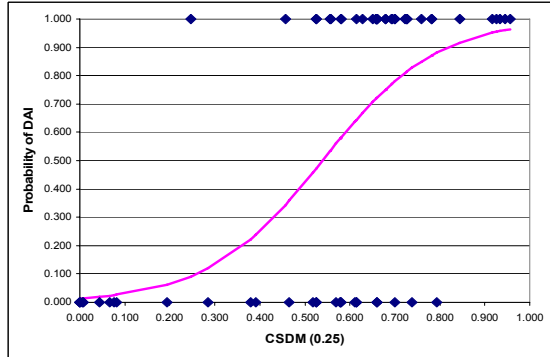


FIGURE 13 a). Probability of DAI versus CSDM (0.25).

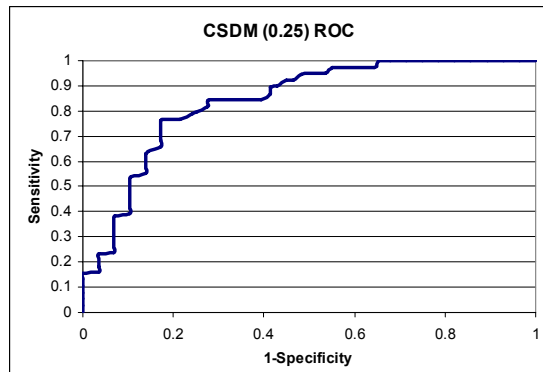


FIGURE 13 b). Receiver Operation Characteristic (ROC) curve for CSDM (0.25).

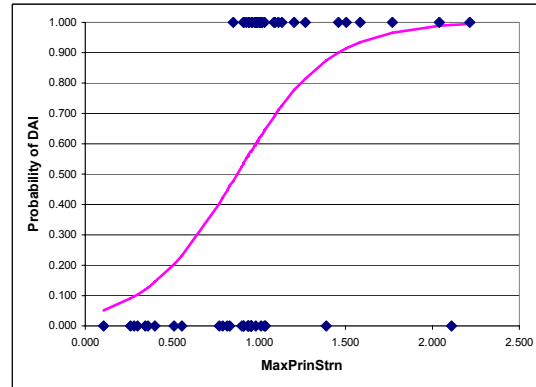


FIGURE 14 a). Probability of DAI versus maximum principal strain.

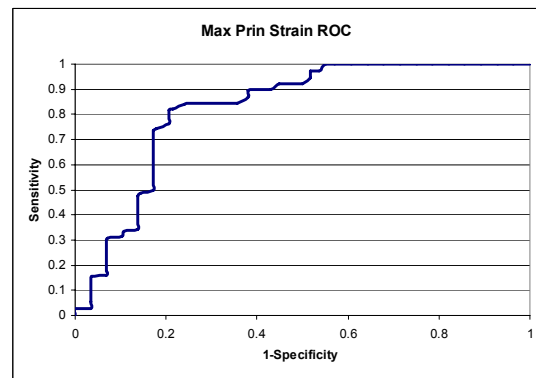


FIGURE 14 b). Receiver Operation Characteristic (ROC) curve for maximum principal strain.

Investigating Potential for TBI in College Football Players

The entire football dataset contains 1712 impacts, of which only 24 were modeled. Figure 15 shows angular acceleration plotted against linear acceleration for every recorded impact. The 24 impacts represent the only impacts where either linear acceleration exceeded 79 g and/or angular acceleration exceeded 5757 rad/s². These nominal thresholds were chosen because they are thought to represent 50% risk of concussion in NFL players (King et al., 2003). Table 4 shows head kinematic parameters for all 24 modeled impacts with their respective injury metrics: CSDM, DDM, RMDM, maximum principal stress, maximum principal strain, and HIC₁₅. It should be noted that none of the 24 impacts resulted in a diagnosed brain injury. Although DDM, RMDM, and maximum principal stress didn't correlate to brain injuries in animal tests, they were still computed for all 24 impacts for the analyses purposes. Linear accelerations in these impacts ranged from 19 g to 135 g. Change in translational velocity, or delta v, ranged from 1.0 m/s

to 5.9 m/s. Angular accelerations ranged from 668 rad/s² to 9919 rad/s². Angular velocities ranged from 4 rad/s to 43 rad/s. Figure 16 presents the results of SIMon FEHM simulations of all 24 impacts. DDM metric is not shown because it was equal to zero for all runs except for one in which it was very small (Table 4). All injury metrics are presented as functions of kinematic measures: linear acceleration (16a), angular acceleration (16b), and angular velocity (16c). For the comparison purposes HIC₁₅ injury metric is also presented. Correlation coefficients are also presented for the injury measures that had an apparent trend with any kinematic measure.

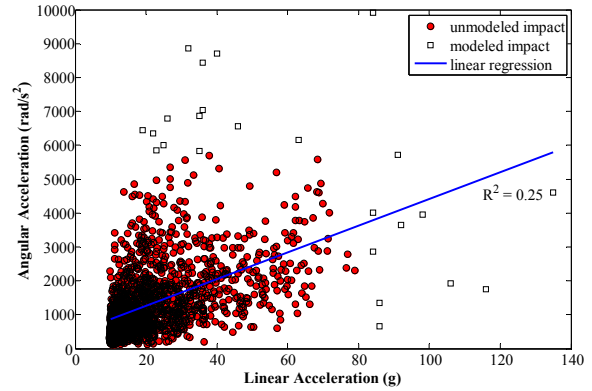


FIGURE 15. Linear acceleration vs. angular acceleration plotted for the entire football dataset of 1712 impacts.

TABLE 4: Kinematics of the 24 modeled impacts sorted by increased linear acceleration and their respective injury metrics.

Case ID	Peak Linear Acceleration (g)	Peak Angular Acceleration (rad/s ²)	Peak Angular Velocity (rad/s)	CSDM (0.25)	Max Principal Stress (MPa)	HIC ₁₅	DDM	RMDM	Max Principal Strain
VT58_a19_r6448	19	6448	27.997	0.069	0.0445	6	0	0.1734	0.677
VT91_a22_r6354	22	6354	25.150	0.070	0.045	8	0	0.1708	0.673
VT58_a23_r5848	23	5848	28.090	0.084	0.047	11	0	0.1775	0.711
VT58_a25_r6000	25	6000	25.700	0.069	0.042	10	0	0.169	0.678
VT72_a26_r6786	26	6786	34.130	0.102	0.055	16	0	0.2011	0.818
VT58_a32_r8866	32	8866	40.840	0.159	0.071	19	0	0.245	0.956
VT66_a35_r5826	35	5826	37.050	0.198	0.103	45	2.7E-06	0.2075	0.921
VT72_a35_r6872	35	6872	29.490	0.087	0.061	31	0	0.198	0.731
VT58_a36_r7037	36	7037	32.600	0.114	0.054	25	0	0.203	0.804
VT58_a36_r8430	36	8430	31.300	0.100	0.062	22	0	0.21	0.781
VT58_a40_r8712	40	8712	39.970	0.162	0.072	36	0	0.238	0.953
VT58_a46_r6567	46	6567	23.140	0.052	0.058	64	0	0.168	0.607
VT82_a63_r6167	63	6167	29.880	0.048	0.059	93	0	0.1731	0.679
VT58_a84_r9922	84	9922	42.510	0.164	0.091	240	0	0.222	0.871
VT82_a84_r2866	84	2866	13.900	0	0.062	205	0	0.0418	0.306
VT82_a84_r4015	84	4015	20.790	0.013	0.063	181	0	0.0746	0.467
VT58_a86_r668	86	668	3.550	0	0.056	209	0	0.01308	0.076
VT71_a86_r1346	86	1346	6.740	0	0.047	175	0	0.0355	0.103
VT58_a91_r5709	91	5709	23.880	0.020	0.069	245	0	0.0699	0.515
VT58_a92_r3646	92	3646	18.900	0.009	0.065	306	0	0.0943	0.464
VT58_a98_r3951	98	3951	15.260	0.001	0.071	264	0	0.072	0.392
VT58_a106_r1917	106	1917	9.540	0	0.233	302	0	0.04927	0.228
VT58_a116_r1759	116	1759	6.140	0	0.075	390	0	0.036	0.15
VT58_a135_r4603	135	4603	17.870	0.001	0.073	555	0	0.077	0.347

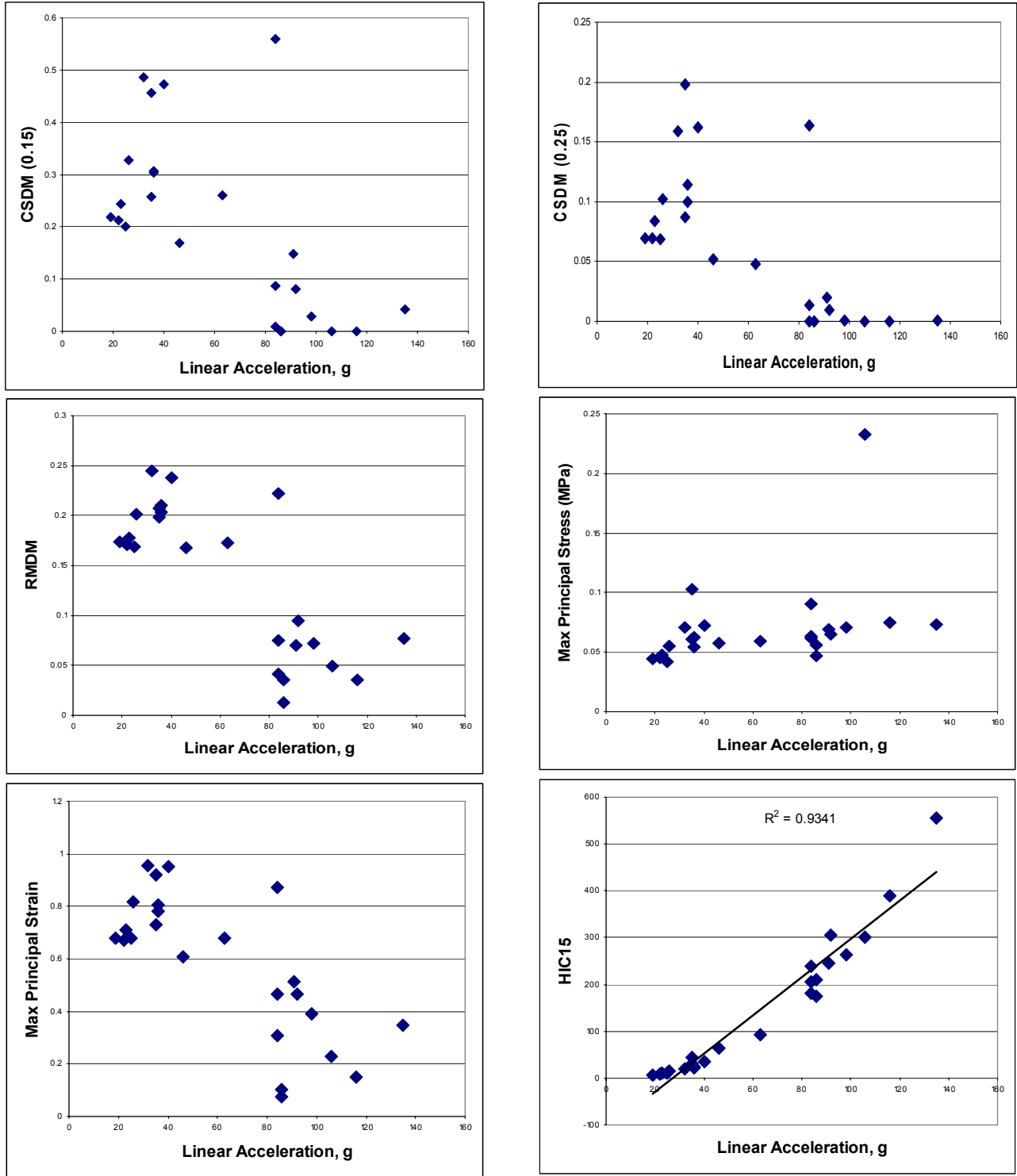


FIGURE 16 a). SIMon FEHM simulations of the college football data: injury metrics versus linear acceleration.

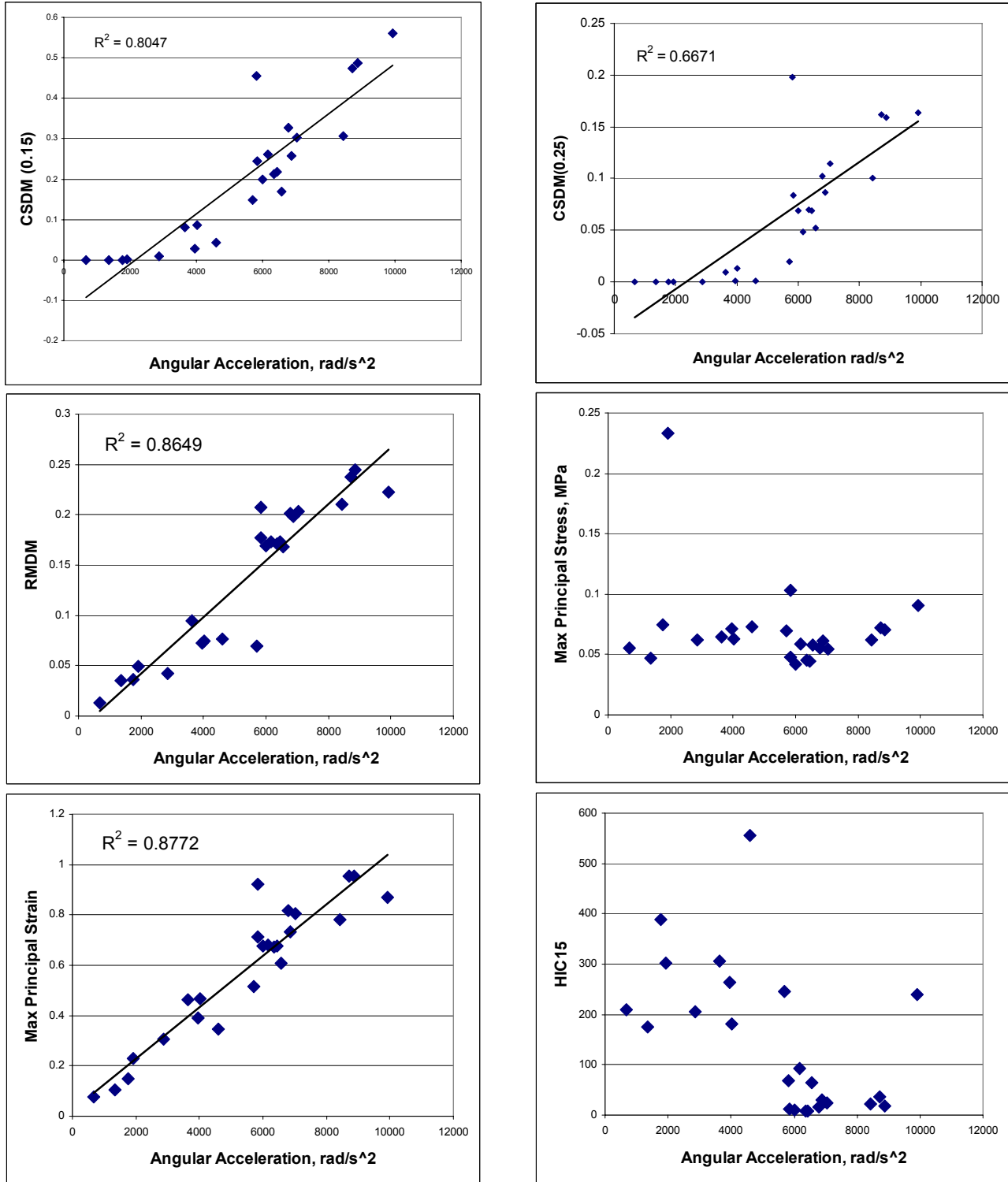


FIGURE 16 b). SIMon FEHM simulations of the college football data: injury metrics versus angular acceleration.

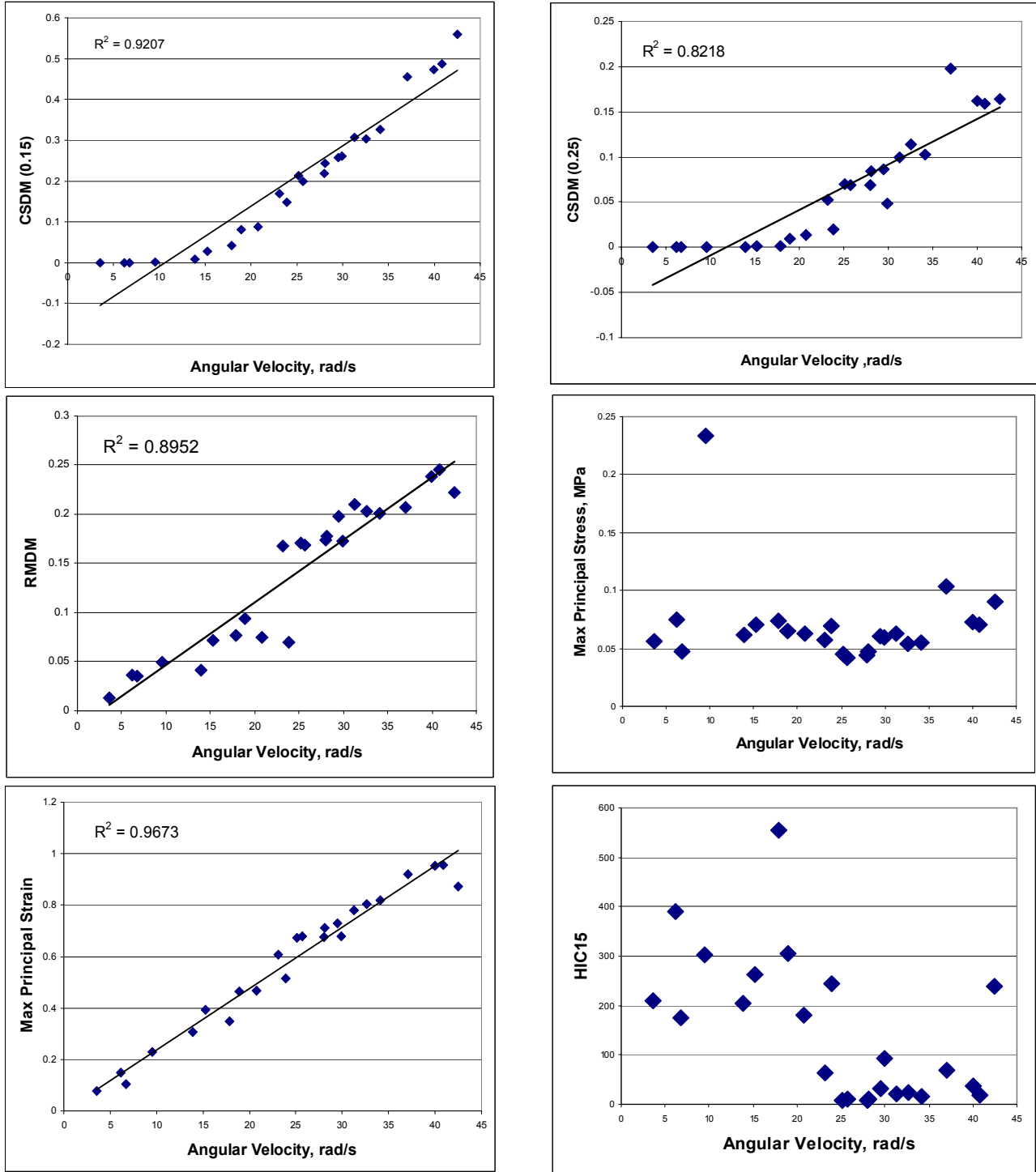


FIGURE 16 c). SIMon FEHM simulations of the college football data: injury metrics versus angular velocity.

TABLE 5: Biomechanical injury metrics for hypothetical frontal and lateral impacts.

Loading Condition	Coronal					Sagittal				
	Max. Prin. Stress (MPa)	Max. Prin. Strain	CSDM 0.25	DDM	RMDM	Max. Prin. Stress (MPa)	Max. Prin. Strain	CSDM 0.25	DDM	RMDM
Peak Lin =200G's Peak Ang =12,000 rad/s ²	0.201	1.75	0.848	0.039	0.467	0.191	1.36	0.8451	0.067	0.0431
Peak Lin =250G's Peak Ang =15,000 rad/s ²	0.236	1.97	0.891	0.059	0.482	0.229	1.38	0.895	0.101	0.0534
Peak Lin =300G's Peak Ang =18,000 rad/s ²	0.259	1.99	0.925	0.116	0.533	0.275	1.54	0.929	0.132	0.0635
Peak Lin =400G's Peak Ang =24,000 rad/s ²	0.288	1.91	0.962	0.344	0.627	0.356	1.94	0.959	0.187	0.0805

Frontal versus Side Impact

Table 5 presents the results of SIMon FEHM simulations for four different hypothetical loading conditions applied in coronal and sagittal planes. Maximum principal stresses, strains, CSDM (0.25), DDM, and RMDM were the output of the model.

NHTSA Conducted Side Impact Tests Evaluation

Table 6 shows computed injury metrics for case 1 and case 2. Several values of principal strain were used to calculate CSDM. For example, CSDM 0.05 indicated the total volume of elements in brain experiencing maximum principal strain of 0.05 and greater at any time during the loading history. The values of CSDM up to maximum principal strain of 0.4 are given for comparison purposes. CSDM (0.25) is given in bold as it represents the injury metric obtained from the animal tests.

DISCUSSION

This manuscript presents a new, geometrically detailed, finite element model of human head developed for use within the concept of SIMon (simulated injury monitor) that takes surrogate head 3-dimensional kinematics as an input (measured elsewhere – ATD or another model), applies it to the undeformable skull of the model, and outputs various brain injury measures. The topology of the model was developed from human CT scans and then compared to that of an average adult male (Figure 3) derived from Procrustes shape analysis of multiple

TABLE 6: Injury metrics for NHTSA conducted side impact cases 1 (with side curtain airbag) and 2 (without side airbag).

Injury Metrics	Case 1	Case 2
CSDM 0.05	0.98334	0.9998
CSDM 0.10	0.7813	0.98465
CSDM 0.15	0.3377	0.9145
CSDM 0.2	0.1252	0.722
CSDM 0.25	0.0478	0.4855
CSDM 0.3	0.0163	0.2926
CSDM 0.35	0.00531	0.1668
CSDM 0.4	0.00142	0.0926
DDM	3.06E-5	0
RMDM	0.0776	0.2006
Max. Principal Stress(MPa)	0.07196	0.0881
Max. Principal Strain	0.5752	0.9202
HIC ₁₅	668	225

cross-sectional CT scans from 59 individuals. The model's topology replicated the shape of average adult human quite well. This topology was used to generate a high quality mesh with a minimum amount of elements. The parts of the model – cerebrum, cerebellum, brainstem, ventricles, CSF and PAC layer, falx, tentorium, and parasagittal blood vessels – were identified and material properties assigned.

Several material models and properties were investigated before the final selection of the Kelvin-Maxwell model with the properties shown in Table 1. The shear stress response of each material model (Figure 6) indicated that the Kelvin-Maxwell model was the softest among those investigated. It also gave the best overall correlation with the experimental data (Hardy et al. 2001, Nahum et al. 1977, Trosseille et al. 1992). Kelvin-Maxwell material model also proved to be more stable in LS-Dyna than Ogden Rubber or linear viscoelastic material models (Figure 8) despite having the softest properties. It is worth mentioning that when the model was run with the Ogden Rubber brain material model with properties taken from Kleiven (2007) the response to the NDT data was similar to the Kelvin-Maxwell model with shear modulus of approximately 10 kPa, and the NDTs displacement magnitudes were approximately an order of magnitude lower than those measured experimentally. It was apparent that the brain material properties must be much softer than those reported by Kleiven (2007) to get the NDTs displacement magnitudes close to those reported by Hardy et al. (2001). The final selection of material constants for Kelvin-Maxwell model (Table 1) was based on the first three parameters of the five-parameter linear viscoelastic model given in Takhounts et al. (2003b). Another deciding factor for selecting Kelvin-Maxwell material model for brain tissue in SIMon FEHM was numerical stability of the model compared to the numerical stability of the model when other material models were used (Figure 8). While the ratio of hourglass to total energy was higher for simulations with Kelvin-Maxwell material model (yet well within the limits recommended by Belytschko 1974, Belytschko and Kennedy 1978, Belytschko and Tsay 1983, Belytschko and Bindeman 1993, Belytschko et al. 2000), the hourglass based deformation modes of the brain modeled with Kelvin-Maxwell material were significantly lower (compare Figure 8a and 8b). The reasons for these differences in the responses are not well understood and their discussion goes beyond the scope of the current study.

The most important evaluating factor for the model's performance was the ability to replicate reasonably the available experimental data: brain NDTs displacement-time histories for three impact scenarios (Hardy et al. 2001) and pressure-time histories at various locations within the brain (Nahum et al. 1977 and Trosseille et al. 1992). It should be noted that these experimental data were generated from five different PMHS with different sizes, ages, etc. They were tested at different times (1977, 1992 and 2001) in different laboratories using different

measuring techniques and different test methods. In other words, there is substantial variability associated with each one of listed above experimental variables that is not reflected in the data and is not yet available. At the same time a single model – SIMon FEHM – was made to fit all the experimental data. As such, one may not expect the model to replicate correctly every single experimental time history. The attention was given to the proper order of magnitude, phasing, and general trend in the data (including experimental data). For example, pressure data for posterior fossa (Nahum et al. 1977) and (Figure 11) doesn't equalize back to zero after the impact is over while pressure measured in other locations does. Also, the pressure gradient was found to be quite high in the model (Figure 11) and, as such, depended highly on the exact location of the sensor that was not reported in Nahum et al. (1977). In the same example of posterior fossa (Figure 11) two computed pressure-time histories from the elements located within the same anatomical region were very close to those measured experimentally for the first pressure wave. Similar conclusions were reached when analyzing experimental and computational data from other pressure tests Trosseille et al. (1992) and Figure 12. Various observations were made when validating the model against the NDT data. First of all, the displacements of the NDTs closest to the boundaries (skull or tentorium) were mostly governed by the local geometry of a particular boundary. Some of the computed displacement-time histories match their experimental counterparts quite well (Figure 9: C755-T2-P5_Z, C755-T2-A3_X, C291-T1-A5_Z, etc.), others match well in magnitudes, but not phase (Figure 9: C755-T2-P5_X, C383-T1-P5_Z, etc.), many have rather poor correlation. Some of these differences can be substantiated with the lack of experimental data necessary for proper validation of the model, others can be attributed to the variability of brain properties in the experimental data, and lack of material properties data for other parts of head (CSF and PAC combined, falx, tentorium, etc). Finally, the differences are due to the modeling errors starting with numerical approximations of physical reality and ending with the integration methods and modeling techniques. Considering all the possible sources of errors the results presented herein are the best that could be obtained when available at this time experimental information was applied to the SIMon FEHM.

Somewhat surprising were results of the animal tests given the fact that rather good correlations of biomechanical injury metrics (CSDM, DDM, and RMDM) with their corresponding injuries (DAI, contusions and focal lesions, ASDH) were obtained

previously using a simplified model of SIMon (Takhounts et al. 2003a). A possible reason for poor DDM and RMDM correlation with contusions and ASDH respectively is the way the contact between the skull and the brain was modeled. In the current version the brain is attached to the combined PAC-CSF layer that, in turn, is attached to the skull, while in the previous “simplified” version a tie-break contact was utilized between both layers. This contact would separate (break) at a set pressure level that affected the pressure distribution within the brain and consequently – DDM, and it also allowed for greater motion of the brain with respect to the skull, thus straining differently the blood vessels and affecting RMDM. Several attempts were made to use the tie-break contact in the current version as well, but due to the more complex topology of the brain and greater amount of elements, the model was not stable. Perhaps, if contusions/focal lesions or ASDH are of research interest, the 2003 version of SIMon FEHM should be used. These findings don’t indicate the superiority of one model over the other, but rather point out the importance of more data with regard to the mechanical properties of the interface between the brain and the skull (PAC-CSF layer) so that a more appropriate modeling approach is utilized in the future. Another surprising result from the animal studies was the magnitude of maximum principal strains computed within the brain. The discussion of the levels of maximum principal strain is given below in the next paragraph.

Head impact data collected from instrumented helmets of college football players has become a very valuable source of information as this is the latest human volunteer head impact data available to date. Although none of the players sustained any reported head injury, the 24 most severe impacts in the 2007 football season simulated in this study, provide information for the safe/non-injurious levels for various injury metrics. In addition, several interesting observations could be made with regard to correlations of biomechanical injury metrics (CSDM, DDM, RMDM, maximum principal stresses and strains) with kinematic parameters (accelerations and velocities). Surprisingly, none of the biomechanical injury metrics correlated with linear acceleration (Figure 16 a), including maximum principal stress. Most of them reduced with increased linear acceleration (CSDM, RMDM, maximum principal strain). Non-surprisingly, HIC_{15} correlated well with linear acceleration as it is a functional of linear acceleration. RMDM and maximum principal strain correlated well with both - angular acceleration and angular velocity (Figure 16 b and c). CSDM was negligible up to a certain level after which it

increased linearly with increased angular acceleration and angular velocity. Three biomechanical injury metrics: CSDM, RMDM, and maximum principal strain correlated a little better with angular velocity than with angular acceleration. RMDM correlated very well with maximum principal strain. Interestingly, maximum principal strain values were as high as 0.96 in two cases. According to many researchers (Bain and Meaney 2000; Morrison III et al. 2003; Lowenhielm 1974; Lee and Haut 1989; Monson 2003; Thibault 1993; Shreiber et al. 1997) the players experiencing these levels of maximum principal strain would sustain DAI (Bain and Meaney 2000; Morrison III et al. 2003), vascular rupture (Lowenhielm 1974; Lee and Haut 1989; Monson 2003), concussion (Thibault 1993), and contusion (Shreiber et al. 1997). None of the players sustained any known brain injuries. This discrepancy could be due to various reasons: (1) soft material properties used to model brain tissue in SIMon FEHM to obtain NDT displacements magnitudes similar to those reported by Hardy et al. (2001); (2) appropriateness of maximum principal strain as a brain injury measure, e.g. CSDM-type criterion may be better as it estimates the volume of brain experiencing a certain strain level; none of the players exceeded CSDM (0.25) critical level of 0.54 established from the animal data; (3) possible errors in measuring angular kinematics in football players. Linear and angular acceleration measurements of helmeted football players were validated through dynamic impact testing with an instrumented Hybrid III head. In an effort to simulate a more realistic interaction between football helmet and Hybrid III head during validation testing, a synthetic skull cap commonly used in football was fitted to the Hybrid III head. The skull cap is composed of 89% nylon and 11% spandex, which substantially reduces friction between the head and helmet when compared to the high coefficient of friction of the Hybrid III skin. This allowed for some sliding of the helmet with respect to the head during testing; however, it is possible that the helmet moves more on a player’s head than on a dummy, and therefore angular accelerations may be overestimated in the field data. Based on the previous experience with a simpler brain model (Takhounts et al. 2003a), it is believed that most of the discrepancies are associated with reason (1). In Takhounts et al. (2003a) the brain constitutive parameters were stiffened up to obtain levels of injurious maximum principal strain comparable to those reported by previous researchers, thus reducing substantially the magnitudes of computed NDTs displacements. The levels of maximum principal strain do not seem to be dependent on the geometry of the model used in the

analysis (simplified or detailed), but depend solely on the material properties used to model brain tissue. Using nonlinear constitutive model, such as Ogden Rubber, doesn't address the discrepancy between the injurious strain levels and NDTs displacements magnitudes. Another interesting observation was that neither HIC_{15} nor maximum principal stress correlated with any angular kinematic parameters. Assuming that biomechanical injury metrics are more realistic indicators of potential for TBI in humans, then neither HIC_{15} nor linear acceleration are applicable in evaluating potential for TBI. Instead, either angular acceleration or angular velocity is better suited for this purpose. This observation is specific to this particular dataset and may change with increased number and severity of impacts.

Interesting trends can be observed when looking at the results of frontal/sagittal versus side/coronal impacts (Table 5). For linear accelerations of up to 250 g and angular accelerations of up to 15,000 rad/s^2 maximum principal stress and maximum principal strain were greater for side/coronal impacts indicating that side impact is more harmful to human brain for this level of loading. With increased magnitudes of linear and angular accelerations, first maximum principal stress becomes greater in frontal/sagittal impact (300 g, 18,000 rad/s^2), then both maximum principal stress and strain become greater in frontal/sagittal impact. CSDM(0.25) in both directions was similar irrespectively of the magnitude of the loading (the difference is in a volume of just a few elements – Table 5). DDM was higher in sagittal plane for loading of up to 300 g and 18,000 rad/s^2 , then became higher in coronal plane – a trend opposite to that of the maximum principal stress. RMDM was an order of magnitude higher in coronal plane for any level of loading. Better trends could have been established if linear and angular kinematics were applied separately rather than in combination with each other. However, it was felt that the combination of linear and angular kinematics better represented realistic impact environment. Regardless of the selection of hypothetical loading conditions, SIMon FEHM showed that coronal/side impact seems to produce greater values of the majority of biomechanical injury metrics when compared to those of the sagittal/frontal impact.

There were no surprises found in the demonstration of the use of SIMon FEHM in the evaluation of NHTSA conducted side impact tests. All the biomechanical injury metrics for case 1 (with side curtain airbag) were much lower than those for case 2 (no side airbag), although HIC_{15} value for case 1 was more than twice greater than it was for case 2. This

example demonstrates the greater ability of SIMon FEHM to isolate potentially harmful environment (case 2) from a relatively safe one (case 1) compared to the existing head injury criteria. Both cases indicate that there is a significant head rotation in side impact scenario. Linear acceleration based injury criteria may not be as effective in this loading scenario as the angular acceleration/velocity based injury criteria.

The necessity and importance of angular head kinematics in evaluating potential for TBI has been discussed in the biomechanical literature since the 1940s (Holbourn 1943, Gennarelli et al. 1972, Ueno and Melvin 1995). This study seems to confirm the original Holbourn hypothesis: translational kinematics of the head is not injurious (based on his 2-dimensional gel model), while rotational head kinematics may explain the majority of TBI due to incompressibility of brain tissue. In other words, the only way to deform/strain a soft, nearly incompressible material (brain) contained within an almost undeformable shell (skull) is to rotate the shell. Translation of the skull does not deform the brain, but rather generate a pressure wave that may be as harmful at higher rates of loading as the excess deformation. Another possible way of deforming the brain is by “pulling” on the brainstem thus creating a motion of the brain through foramen magnum and straining the brain. This could occur during hyper extension/flexion of the neck. This mode of potential brain deformation was not considered in this study and, perhaps, should be investigated in the future.

Limitations of this (or any other) model can be grouped into two categories: 1) lack of the experimental data to thoroughly validate the model and to establish biomechanically based injury criteria, and 2) numerous mathematical approximations necessary to replicate the physical system. To improve the first category of limitations more experimental data is necessary to establish statistical performance corridors for NDTs and pressure within the brain. To address inhomogeneity and anisotropy of modeled tissue, more constitutive information is necessary. The injury criteria should be verified using tissue based human brain injury data. Improvements in the second category of limitations go beyond the scope of biomechanical research. These improvements, however, should be closely monitored by the biomechanical modeling community and implemented in the future mathematical models as they become available.

CONCLUSIONS

A new, more geometrically detailed, SIMon FEHM was developed, validated, and used in investigation of potential for TBI in American college football players, comparison of injury measures in hypothetical frontal versus side impacts, and analysis of two different NHTSA conducted side impact tests.

Based on the simulation results of SIMon FEHM several observations were made:

- CSDM (0.25) and maximum principal strain correlated well with DAI observed from previously conducted animal tests; DDM didn't correlate to contusions or focal lesions, and RMDM didn't correlate with ASDH; maximum principal stress didn't correlate to any type of TBI in animals.
- Biomechanical injury measures correlated better with angular acceleration and angular velocity, but not with linear acceleration in the simulated 24 football players impacts.
- Maximum principal stress didn't correlate with any kinematic measure.
- Maximum principal strain correlated well with RMDM. The values of maximum principal strain in most simulated cases of uninjured college football data and animal tests were high compared to those reported previously to be injurious.
- For the hypothetical loading scenarios the majority of biomechanical injury parameters indicated that side/coronal impact was more harmful to the head than frontal/sagittal impact.
- SIMon FEHM predicted that a side curtain airbag reduced the potential for brain injury in a side impact crash. The linear acceleration-based criterion, HIC₁₅, was not able to predict this reduction.
- The results strongly suggest that an angular injury criteria better predict traumatic brain injury than linear acceleration based injury criteria.
- The study is limited to the current knowledge of experimental data and modeling techniques.

ACKNOWLEDGMENTS

The authors would like to acknowledge the guidance and helpful advice of Dr. Rolf Eppinger (retired) who is the true inventor of the concept of simulated injury monitor (SIMon), and the mechanical equivalents (CSDM, DDM, and RMDM) of most frequently

occurring TBI (DAI, contusions and focal lesions, and ASDH). This paper would not have been possible without his inventions. Also, the authors gratefully acknowledge Toyota Central Research and Development Labs, and the National Institutes of Health (NINDS) contract R01HD048638 for sponsoring parts of the project related to collecting college football data.

REFERENCES

- Abel, J., Gennarelli, T.A., Seagawa, H. (1978) In cadence and severity of cerebral concussion in the rhesus monkey following sagittal plane angular acceleration. Proc. 22nd Stapp Car Crash Conference, pp. 33-53, Society of Automotive Engineers, Warrendale, PA.
- Arbogast, K. B., Meaney, D. F., and Thibault, L. E. (1995) Biomechanical characterization of the constitutive relationship for the brainstem. Proc. 39th Stapp Car Crash Conference, pp. 153-159, Society of Automotive Engineers, Warrendale, PA.
- Bain A.C., Meaney D.F. (2000) Tissue-level thresholds for axonal damage in an experimental model of central nervous system white matter injury. *J Biomech Eng.* 122(6): 615-22.
- Bandak, F.A., and Eppinger, R.H. (1995) A three-dimensional finite element analysis of the human brain under combined rotational and translational acceleration. Proc. 38th Stapp Car Crash Conference, pp. 145-163. Society of Automotive Engineers, Warrendale, PA.
- Bandak, F.A., Zhang, A. X., Tannous, R. E., DiMasi, F., Masiello, P., Eppinger, R., (2001) Simon: a simulated injury monitor; application to head injury assessment. ESV 17th International Technical Conference on the Enhanced Safety of Vehicles, National Highway Traffic Safety Administration, Washington, DC.
- Belytschko, T.B. (1974) Finite element approach to hydrodynamics and mesh stabilization. In *Computation Methods in Nonlinear Mechanics*, ed. Oden, J.T. et al. The Texas Institute for Computational Mechanics.
- Belytschko, T.B., Liu W.K. and Moran B. (2000) *Nonlinear Finite elements for Continua and Structures*, John Wiley & Sons, Chichester, U.K.
- Belytschko, T.B. and Kennedy, J.M. (1978) Computer models for subassembly simulation. *Nucl. Engng. Des.* 49: 17-38.

- Belytschko, T.B. and Tsay, C.S. (1983). A Stabilization Procedure for the Quadrilateral Plate Element with One-Point Quadrature, *International Journal for Numerical Methods in Engineering*, Volume 19, 405-420.
- Belytschko, T.B. and Bindeman, L.P. (1993) Assumed Strain Stabilization of the Eight Node Hexahedral Element, *Computer Methods in Applied Mechanics and Engineering*, Volume 105, 225-260.
- Bilston, L. E., Liu, Z., Phan-Thien, N. (1998) Linear viscoelastic properties of bovine brain tissue in shear. *Biorheology* 34(6), 377-385.
- Bookstein, F. L. (1996). Biometrics, biomathematics and the morphometric synthesis. *Bull Math Biol.* 58(2): 313-65.
- Bookstein, F. L. (1997). Landmark methods for forms without landmarks: morphometrics of group difference in outline shape. *Medical Image Analysis* 1(number 3): 225-243.
- CDC, National Center for Injury Prevention and Control, 'Traumatic Brain Injury Facts', <http://www.cdc.gov/ncipc/factsheets/tbi.htm>, 2003.
- Chu, J. J., Beckwith, J. G., Crisco, J. J., and Greenwald, R. (2006) A Novel Algorithm to Measure Linear and Rotational Head Acceleration Using Single-Axis Accelerometers. in *World Congress of Biomechanics*, Munich, Germany.
- Danelson, K.A., Loftis, K.L., Yu, M.M., Gayzik, F.S., Geer, C.P., Slice, D.E., Stitzel, J.D.. (2008) Geometric Shape Scaling Factors for the Pediatric Brain Based on Morphometric Analysis,"SAE Digital Human Modeling.
- Darvish, K.K., Crandall, J.R. (2001) Nonlinear viscoelastic effects in oscillatory shear deformation of brain tissue. *Medical Engineering and Physics* 23: 633-645.
- Donnelly, B. R. and Medige, J. (1997) Shear properties of human brain tissue. *J. Biomech. Engng* 119, 423-432.
- Eigen, A. M. and Martin, P. G. (2005) Identification of real world injury patterns in aid of dummy development. 19th Enhanced Safety of Vehicles.
- Estes, M. S. and McElhaney, J. H. (1970) Response of brain tissue of compressive loading. *ASME*, No. 70-BHF-13.
- Fallenstein, G. T., Hulce, V. D., and Melvin, J. W. (1969a) Dynamic material properties of human brain tissue. *J. Biomechanics* 2, 217-226.
- Fallenstein, G. T., Hulce, V. D., and Melvin, J. W. (1969b) Dynamic material properties of human brain tissue. *ASME*, No. 69-BHF-6.
- Galford, J. E., and McElhaney, J. H. (1969) A Viscoelastic Study of Scalp, Brain, and Dura. *J. Biomechanics* 3, 211-221.
- Gennarelli, T.A., Thibault, L.E., and Ommaya, A.K. (1972) Pathophysiologic Responses to Rotational and Translational Accelerations of the Head. *Stapp Car Crash Journal* 16: 296-308.
- Gennarelli, T.A., Thibault, L.E., Adams, J.H., Graham, D.I., Thompson, C.J., and Marcincin, R.P. (1982a) Diffuse axonal injury and traumatic coma in the primate. *Annals of Neurology* 12(6): 564-574.
- Gennarelli, T.A. and Thibault, L.E. (1982b) Biomechanics of acute subdural hematoma. *J. Trauma* 22(8): 680-686.
- Good, P. (2000) *Permutation Tests: A Practical Guide to Resampling Methods for Testing Hypothesis*. New York, NY, Springer.
- Gunz, P., Mitteroecker P., and Bookstein F. L. (2005) Semilandmarks in Three Dimensions, Pages 73-98 in D. E. Slice, ed. *Modern Morphometrics in Physical Anthropology. Developments in Primatology: Progress and Prospects*. New York, Plenum Publishers.
- Hardy, W.N., Foster, C., Mason, M., Yang, K., King, A., Tashman, S. (2001) Investigation of head injury mechanisms using neutral density technology and high-speed biplanar X-ray. *Stapp Car Crash Journal* 45: 337-368.
- Haut, R.C. and Lee, M.C. (1989) Insensitivity of tensile failure properties of human bridging veins to strain rate: implications in biomechanics of subdural hematoma. *Journal of Biomech.* 22(6-7):537-42.
- Hodgson VR, Gurdjian ES, Thomas LM. (1966) Experimental skull deformation and brain displacement demonstrated by flash x-ray technique. *Journal of Neurosurgery*. Nov, 25(5):549-52.
- Holbourn, A.H.S. (1943) Mechanics of head injury. *Lancet* 2, October 9: 438-441.

- King AI, Yang KH, Zhang L, Hardy W and Viano DC. (2003) Is Head Injury Caused by Linear or Angular Acceleration? Proceedings of the International Research Conference on the Biomechanics of Impact (IRCOBI): Lisbon, Portugal.
- Kleiven, S. and Hardy, W.N. (2002) Correlation of an FE model of the human head with local brain motion-consequences for injury prediction. *Stapp Car Crash Journal* 46: 123-144.
- Kleiven, S. (2007) Predictors for Traumatic Brain Injuries Evaluated through Accident Reconstructions. *Stapp Car Crash Journal* 51: 81-114.
- Koeneman, J. B. (1966) Viscoelastic properties of brain tissue. Unpublished M.S. thesis, Case Institute of Technology.
- Lee, M.C., and Haut, R.C. (1989) Insensitivity of tensile failure properties of human bridging veins to strain rate: Implications in biomechanics of subdural hematoma. *J. Biomech.* 22(6/7): 537-542.
- Levchakov, A., Linder-Ganz, E., Raghupathi, R., Margulies, S.S., and Gefen, A. (2006) Computational studies of strain exposures in neonate and mature rat brains during closed head impact. *J. Neurotrauma* 23(10):1570-1580.
- Ljung, C. (1975) A model for brain deformation due to rotation of the skull. *J. Biomechanics* 8, 263-274.
- Lowenhielm, P. (1974) Dynamic properties of the parasagittal bridging veins, *Z. Rechtsmedizin* 74: 55-62.
- LS-DYNA Keyword User's Manual (2007), Version 971, Livermore Software Technology Corporation, Livermore, CA.
- Manoogian, S., McNeely, D., Duma, S., Brolinson, G., and Greenwald, R. (2006) Head acceleration is less than 10 percent of helmet acceleration in football impacts. *Biomed Sci Instrum*, vol. 42: 383-388.
- Meaney, D.F, Smith, D., Ross, D.T., and Gennarelli, T.A. (1993) Diffuse axonal injury in the miniature pig: Biomechanical development and injury threshold. *ASME Crashworthiness and occupant protection in transportation systems* 25: 169-175.
- Miller, K. and Chinzei, K. (1997) Constitutive modeling of brain tissue: experiment and theory. *J. Biomechanics* 11/12, 1115-1121.
- Monson, K.L. (2003) Axial mechanical properties of fresh human cerebral blood vessels. *J. Biomech Eng.* 2003 Apr, 125(2): 288-294.
- Morrison III, B., Carter, H.L., Wang, C.C.B., Thomas, F.C., Hung, C.T., Ateshian, G.A. and Sundstrom, L.E. (2003) A tissue tolerance criterion for living brain developed in an in-vitro model of traumatic mechanical loading. *Stapp Car Crash Journal*, 47: 93-105.
- Nahum, A. M., Smith, R., Ward, C. C., (1977) Intracranial pressure dynamics during head impact. *Stapp Car Crash Journal* 21: 339-366.
- Nicolle, S., Lounis, M., Willinger, R. (2004) Shear properties of brain tissue over a frequency range relevant for automotive impact situations: New experimental results. *48th Stapp Car Crash Journal*: 239-258.
- Nusholtz, G.S., Lux, P., Kaiker, P., and Janicki, M.A., (1984) Head impact response skull deformation and angular accelerations. *Proc. 28th Stapp Car Crash Conference*, pp. 41-74, Society of Automotive Engineers, Warrendale, PA.
- Nusholtz, G.S., Wylie, B., and Glascoe, L.G. (1995) Cavitation/boundary effects in a simple head impact model, *Aviation Space & Environmental Medicine* 66(7): 661-667.
- Ruan, J.S., Khalil, T., King, A.I. (1993) Finite element modeling of direct head impact. *Proc. 37th Stapp Car Crash Conference*, pp. 69-81. Society of Automotive Engineers, Warrendale, PA.
- Rutland-Brown, W., Langlois, J.A., Thomas, K.E., and Xi, Y.L. (2006) Incidence of traumatic brain injury in the United States, 2003. *J. Head Trauma Rehabil.* 21(6):544-548.
- Shreiber, D.I., Bain, A.C. and Meaney, D.F. (1997) In vivo thresholds for mechanical injury to the blood-brain barrier. *41st Stapp Car Crash Conf.*, SAE: 177-190.
- Slice, D. (2005). *Modern Morphometrics. Modern Morphometrics in Physical Anthropology*. D. Slice. New York, Plenum Publishers: 1-45.
- Slice, D. and J. Stitzel (2004). *Landmark-based Geometric Morphometrics and the Study of Allometry*. SAE.
- Stalnaker, R.L., Alem, N.M., Benson, J.B., Melvin, J.W. (1977) Validation studies for head impact injury model. Final report DOT HS-802 566, National Highway Traffic Safety Administration,

- US, Department of Transportation, Washington, DC.
- Shuck, L. and S.H. Advani (1972). Rheological Response of Human Brain Tissue in Shear. ASME Journal of Basic Engineering, 94: p. 905-11.
- Takhounts, E.G., Eppinger, R.H., Campbell, J.Q., Tannous, R.E., Power, E.D., Shook, L.S. (2003a) On the Development of the SIMon Finite Element Head Model. Stapp Car Crash Journal 47: 107-133.
- Takhounts, E.G., Crandall, J.R., Darvish, K.K. (2003b) On the importance of nonlinearity of brain tissue under large deformations. Stapp Car Crash Journal 47:79-92.
- Thibault, L.E., Galbraith, J.A., Thompson, C.J., Gennarelli, T.A. (1981) The effects of high strain rate uniaxial extension on the electrophysiology of isolated neural tissue. ASME Advances in Bioengineering: 211-214.
- Thibault, L.E. (1993) Brain injury from the macro to the micro level and back again: What we have learned to date? Proc. IRCOBI Conf., Eindhoven, The Netherlands: 3-25.
- Trosseille et. al., (1992) Development of a F.E.M. of the human head according to a specific test protocol, Stapp Car Crash 36: 235–253.
- Ueno, K., and Melvin, J.W. (1995) Finite element model study of head impact based on hybrid III head acceleration: The effects of rotational and translational accelerations. J. Biomech Eng. 117(3): 319-328.
- Zhang, L., Yang, K.H., Dwarampudi, R., Omori, K., Li, T., Chang, K., Hardy, W.N., Khalil, T.B., King, A.I. (2001) Recent advances in brain injury research: a new human head model development and validation. Stapp Car Crash Journal 45: 369-394.

